Organic Geochemistry 122 (2018) 147–160

Contents lists available at ScienceDirect

Organic Geochemistry

journal homepage: www.elsevier.com/locate/orggeochem

Wax lipids in fresh and charred anatomical parts of the *Celtis australis* tree: Insights on paleofire interpretation

Margarita Jambrina-Enríquez *, Antonio V. Herrera-Herrera, Carolina Mallol

Archaeological Micromorphology and Biomarker Research Lab, Instituto Universitario de Bio-Orgánica Antonio González, Universidad de La Laguna, Avda. Astrofísico Fco. Sánchez, 2, 38206 La Laguna, Tenerife, Spain

ARTICLE INFO

Article history:
Received 28 January 2018
Received in revised form 18 May 2018
Accepted 30 May 2018
Available online 31 May 2018

Keywords:
n-Alkanes
Fatty acid
Aromatics
Carbon isotopes
Compound-specific isotopes
Plant biomarkers
Wood
Paleofire
Combustion structure

ABSTRACT

Leaf waxes have been assumed to be the dominant source of wax delivered to sediment. However, wooden branches and twigs have not been widely considered in this context and could be a potential source of wax lipids in fire places or combustion structures. Black sedimentary layers are the main material of open-air archaeological combustion structures and represent either carbonized fuel (wood) or the charred ground beneath the fire (mainly leaves) and it is difficult to discern between the two sources. To identify different plant parts as components of combustion residues, fresh and charred leaves, branches and twigs (bark and xylem) of the *Celtis australis* tree were analyzed for aliphatic and aromatic hydrocarbons and fatty acid concentrations, as well as the carbon isotopic composition of *n*-alkanes ($\delta^{13}C_{alkane}$). Charred biomass was produced under limited oxygen conditions at 150, 250 (3 and 5 h), 350 and 450 °C for 1 h. The *n*-alkyl profiles in different parts of *C. australis* are sufficiently distinct to allow their identification as components of combustion structures under low combustion temperature conditions. Average chain lengths and carbon preference index ratios decrease with increasing temperature and vary among plant parts. The $\delta^{13}C_{alkane}$ values remained slightly unaltered up to 350 °C and changed by 3–4‰ at 450 °C. Our results provide new information on the molecular and isotopic changes that occur upon burning different plant parts, which in turn show potential for good preservation of organic matter in archaeological black layers and for positive identification of burned leaf and wood residues in them.

1. Introduction

Wax lipids constitute an important part of the organic components in plants and include *n*-alkanes and *n*-alkanoic (fatty) acids. They are found in plant cuticles and their composition and abundance vary among species, between tissues and with ontogeny (Wiesenberg et al., 2004; Diefendorf et al., 2011; Diefendorf and Freimuth, 2017). Different *n*-alkane compositions and concentrations have been found among plant parts such as leaves, stems, roots, flowers and fruits (Dove et al., 1996; Smith et al., 2001; Wiesenberg et al., 2004; Jansen et al., 2007; Huang et al., 2011; Gocke et al., 2011; Gamarra and Kahmen, 2015). Although lipid composition (alkanes, fatty acids) of woody tissues such as roots and stems from herbs, grasses and shrubs (Wiesenberg et al., 2004; Wiesenberg and Schwark, 2006; Huang et al., 2011; Gocke et al., 2011; Gamarra and Kahmen, 2015) and wood (branches and wood cores) from trees (O'Malley et al., 1997; Adams and Wright, 2012; Knicker et al., 2013) have been previously documented, only a few studies have investigated the lipid composition of the bark and xylem in fresh and buried tree wood (e.g., steroids and triterpenoids, Schnell et al., 2014) or the volatile constituents of shrub stems (aliphatic hydrocarbons, alcohols, ketones, fatty acids and terpenes, Mastelic et al., 2006).

Within the wax components, *n*-alkanes have greater resistance to microbial degradation than lipid precursor compounds like fatty acids (Cranwell, 1981) which makes them suitable for use as higher plant biomarkers to reconstruct past vegetation histories and climate change from sediment inventories (Meyers, 2003). Although the concentration of *n*-alkanes is higher in leaves and stems (e.g., Gocke et al., 2011; Gamarra and Kahmen, 2015); roots of selected species of grasses can contribute *n*-alkanes to the soil (e.g., arrowgrass species, Gocke et al., 2011). In archaeological combustion structures (fire places), which involve wood as a common fuel due to its optimal pyrogenic properties (Braadbaart and Poole, 2008), branches or wood are likely to be potential sources of *n*-alkane signals in surface soils.

The molecular composition of fine particles emitted from biomass and wood burning has been widely studied in aerosols (e.g., Fine et al., 2001; Oros and Simoneit, 2001a, b; Simoneit,

* Corresponding author.
E-mail address: mjambrin@ull.edu.es (M. Jambrina-Enríquez).

https://doi.org/10.1016/j.orggeochem.2018.05.017
0146-6380/

2002) as well as molecular markers of biochar (e.g., Kuo et al., 2008; Kaal et al., 2012; Keiluweit et al., 2012; Wiedemeier et al., 2015) and fossil charcoal (e.g., Marynowski et al., 2014). Schnell et al. (2014) reported the molecular composition (steroids and triterpenoids) of fresh and archaeological buried wood remains. Molecular studies in buried ancient topsoil containing charred organic matter (OM) (e.g., Eckmeier and Wiesenberg, 2009) and in hearths (archaeological combustion structures, Mallol et al., 2013, March, 2013; burnt bedding, Collins et al., 2017) focused on *n*-alkanes due to their high preservation potential (Cranwell, 1981).

A well preserved in situ archaeological combustion structure may comprise a sedimentary stratified sequence made up of a reddish-brown layer at the base (combustion substrate: thermally altered soil and sediment), overlain by a dark brown/black layer (combustion substrate: fuel or charred topsoil) and capped by a white/yellowish layer (combustion residues: wood or grass ash) (Mallol et al., 2017). The black sedimentary layer is normally considered as representing either partially combusted or carbonized fuel (Leroi-Gourhan, 1973) or the charred ground beneath the fire (Mallol et al., 2013) and it is difficult to discern between the two sources. During the last few years, a number of studies have been devoted to the investigation of molecular biomarkers in experimental and archaeological combustion structures (e.g., Mallol et al., 2013, March, 2013) underlining the potential of charred OM to preserve biomarker fingerprints over a long time scale. Experimental data has shown that the average temperatures associated with black sedimentary layers – below 300 °C – are high enough for the charring of organic compounds and to make them unappealing to biodegrading soil fauna, but not as high as to destroy their lipid biomarker chemical fingerprints, specifically *n*-alkanes (Mallol et al., 2013). In this regard, the lipid composition of modern charred leaves (*n*-alkanes and fatty acids), wood (bark and xylem) and twigs (bark and xylem), under laboratory-controlled conditions could be used as a reference to assess that black sedimentary layers representing the charred ground beneath the fire and not exclusively the carbonized wood fuel and to explore variation in lipid composition with increasing temperature. Only for cases without OM in the substrate (red inorganic layers directly below ash) the experimental data have shown higher temperatures (Aldeias et al., 2016). Although the concentration of *n*-alkanes in leaves is higher than in other plant tissues (e.g., Gamarra and Kahmen, 2015; Diefendorf and Freimuth, 2017), some authors have recently suggested that roots could contribute significant amounts to the topsoil as well (Jansen and Wiesenberg, 2017). However, compared to leaves, the concentration of *n*-alkanes released by roots is one or more orders of magnitude lower (e.g., Gamarra and Kahmen, 2015; Jansen and Wiesenberg, 2017).

Concerning the effects of temperature on lipid composition, it has been demonstrated that charring protects OM from oxidation and microbial activity (Braadbaart and Poole, 2008; de La Rosa and Knicker, 2011) and that *n*-alkanes are resistant to heat (Fernández et al., 1997; Campo et al., 2011). During charring (incomplete combustion of OM under limited oxygen conditions and between 150 and 500 °C, Ellis, 1959; Braadbaart and Poole, 2008), the chemical composition and the molecular and structural configuration of OM undergo thermal modification. Thermal degradation of plant biomass at low temperatures (≤350 °C) under laboratory-controlled conditions have shown that at ≤300 °C, the *n*-alkane distribution still exhibits a strong odd-over-even carbon chain predominance (Wiesenberg et al., 2009; Diefendorf et al., 2015), the *n*-alkane carbon isotope values remain unaltered (Diefendorf et al., 2015) and simple aromatic compounds are present at temperatures close to 250–300 °C (Wiesenberg et al., 2009; Wiedemeier et al., 2015). At ~300–350 °C, incomplete combustion–induced thermal breakdown of long chain *n*-alkanes produce short chain homologues and an even-over-odd carbon number predominance (Wiesenberg et al., 2009; Knicker et al., 2013; Diefendorf et al., 2015), the *n*-alkane carbon isotope ratios shift (Diefendorf et al., 2015) and aromaticity increases (Wiesenberg et al., 2009; Wiedemeier et al., 2015).

To assess the source biomass and degree of degradation, previous studies have used molecular ratios such as average chain length (ACL), which is the weighted average of the various carbon chain lengths (Cranwell, 1973) and carbon preference index (CPI), which captures the ratio of odd- to even-carbon numbered alkanes (Bray and Evans, 1961). Although the ACL has been used to differentiate between OM derived from woody and non-woody plants (Cranwell, 1973), recent studies on modern plants do not show a significant difference between the two types and ACL variation is considered to respond mainly to variation in temperature and humidity (Wang et al., 2015; Bush and McInerney, 2015). The CPI ratio discriminates between OM derived from higher plants (CPI values > 5) and bacteria and algae (CPI ~ 1) (Eglinton and Hamilton, 1967; Cranwell, 1981; Rieley et al., 1991) and is also used as a proxy for the degree of OM degradation (Bray and Evans, 1961). However, CPI values could also be influenced by climatic factors (Sachse et al., 2004). Concerning charred OM, the ACL and CPI were found to be useful markers for incomplete burning of biomass with lower ACL and CPI values at combustion temperatures ≥300 °C (Wiesenberg et al., 2009; Knicker et al., 2013; Diefendorf et al., 2015).

In addition to the above-mentioned organic biomarkers, stable carbon isotopes in alkanes can reveal valuable information about the relative contributions of C3 (Calvin-Benson cycle) versus C4 plants (Hatch-Slack cycle), as C3 plants have $\delta^{13}C$ values in the range of –31‰ to –39‰, while C4 plants have $\delta^{13}C$ values in the range of −18‰ to −25‰ (e.g., Diefendorf and Freimuth, 2017). Moreover, compound-specific carbon isotope analysis in charred OM can provide insight into the effect of thermal maturation in leaf wax *n*-alkyl components (e.g., Diefendorf et al., 2015).

With the assumption that the *n*-alkane distribution of modern plant species are representative of past plant assemblages (e.g., Schwark et al., 2002), leaves, branches (bark and xylem-wood) and twigs (bark and xylem) from a living tree (*Celtis australis* L.), were analyzed to identify potential sources of the charred (organic) residues of open-air archaeological black sedimentary layers, i.e. carbonized fuel (wood and twigs) or charred fine OM derived from the soil substrate (mainly leaves). To corroborate that the black sedimentary layers represent charred soil matter beneath the fire (e.g., leaves, seeds, roots), *C. australis* tree was selected for study given that the presence of calcitic *Celtis* seed coats have been reported in sediment associated with Pleistocene archaeological combustion structures (Mallol et al., 2013) as well as in sediment from several other Pleistocene archaeological sites (Messager et al., 2010; García Moreno et al., 2014; Allué et al., 2015), while no wood has been identified in the anthracological record (e.g., Vidal-Matutano et al., 2018). Given that the lipid composition of *Celtis* seeds has been widely studied due to their nutritional and physicochemical properties (Demır et al., 2002; Badoni et al., 2010; Ota et al., 2017), and based on the typically low concentrations of *n*-alkanes in roots previously reported (e.g., Gocke et al., 2011; Gamarra and Kahmen, 2015), this study is focused on leaves and wood. For a better understanding of the role and process of thermal alteration in plants, charred biomass of different anatomical parts of *C. australis* was produced under limited oxygen conditions at different temperatures (150, 250, 350 and 450 °C) and the compositions of charred materials were analyzed for aliphatic and aromatic hydrocarbons and fatty acids. To further investigate the influence of combustion duration the reference materials were also heated at 250 °C (average temperatures associated with black

sedimentary layers of experimental combustion structures are below 300 °C, Mallol et al., 2013) for a scheduled period (1, 3 and 5 h). Molecular signatures were used in combination with compound–specific isotopic analysis of individual alkanes ($\delta^{13}C_{alkane}$) to explore possible changes occurring during thermal degradation. This study explores the potential of molecular and carbon isotope signatures of *n*-alkyl lipids in charred anatomical parts of *C. australis* to determine the source of different charred residues from open-air archaeological black sedimentary layers.

2. Materials and methods

2.1. Samples

Different anatomical fractions (i.e. leaves, branches and twigs) of *Celtis australis* L. were collected in July 2015 (leaf samples) and April 2016 (branch and twig samples) near the archaeological site of El Salt (Alcoy, Spain) (38°41′14″N, 0°30′32″W, 726 m above sea level). *C. australis*, commonly known as nettle tree or European hackberry, is a deciduous tree native to the Mediterranean Region traditionally placed in the Ulmaceae family (Tutin et al., 1964) and later re-classified into the Cannabaceae family (Sytsma et al., 2002). The leaf, branch (3 cm diameter) and twig (1 cm diameter) samples were collected 2 m above the ground, rinsed with distilled water to eliminate any extraneous materials and oven dried at 60 °C over 24 h (e.g., Gamarra and Kahmen, 2015).

2.2. Charring

The leaf (4 g) samples were cut into small pieces (1 cm length) and the branches (20 g) and twigs (20 g) in pieces of 2 cm length. All the samples were heated in a ceramic crucible with a diameter of 4.2 cm and a height of 2.5 cm and wrapped with Al foil to limit O_2 supply during charring (e.g., Wiesenberg et al., 2009; Wiedemeier et al., 2015). All the samples were heated and held for 1 h at four different temperatures (150 °C; 250 °C; 350 °C and 450 °C) in a muffle furnace, with a ramp rate of 26 °C/min (Kuo et al., 2008). In addition, leaf samples were also heated and held at 250 °C for a scheduled period (1 h, 3 h and 5 h) to explore the influence of combustion duration. After combustion, the samples were cooled down in the closed furnace overnight and subsequently milled to a fine powder before their analysis.

2.3. Lipid extraction, analysis and quantification

Non-volumetric material (including glassware and glass wool) was calcined at 450 °C during 10 h before extraction to eliminate any possible organic compounds. Lipid extraction was accomplished using a modified version of a previously published methodology (Bhattacharya et al., 2017). Lipids were extracted from fresh and charred leaf samples (0.3–0.5 g), branches and twigs (1–2 g) with dichloromethane/methanol (DCM:MeOH, 9:1, v:v) (10–20 mL) by ultrasonic extraction (3 × 30 min) at controlled temperatures below 30 °C, followed by centrifugation (3 × 10 min at 4700 rpm) and finally filtered through annealed glass wool (Rushdi et al., 2014, 2018).

The total lipid extract was separated into six fractions of different polarity using a 2 mL solid phase column filled with glass wool, 0.1 g pure quartz sand (50–70 mesh) and 1 g of activated silica (70–230 mesh), previously calcined at 450 °C over 10 h. The solid phase columns were preconditioned with one portion of hexane corresponding to the dead volume (DV, 1.5 mL). Fraction 1 (F1: *n*-alkanes) eluted with 3/8 of DV in hexane (562 μL), fraction 2 (F2: aromatics) with 2DV in hexane:DCM (8:2, v:v) (3 mL), fraction 3 (F3: ketones) with 2DV in DCM (3 mL), fraction 4 (F4: *n*-alkanols) with 2DV in DCM/ethyl acetate (EtOAc) (1:1, v:v) (3 mL) and fraction 5 (F5: acids and diols) with 2DV in EtOAc (3 mL). All the fractions were dried under a N_2 flow in an Organomation evaporator. After addition of internal standard (IS) 5α-androstane (2000 mg/L in DCM, purity ≥99.9%, Sigma-Aldrich) 8 mg/L in F1 and F2, the volume was topped with 1 mL of DMC (F1: fresh leaf samples), 150 μL of DCM (F1: fresh and charred samples) or 50 μL of DCM (F2: fresh and charred samples).

For the determination of fatty acids, F5 was methylated and converted into fatty acid methyl esters (FAMEs) (Liu, 1994). Fraction 5 was redissolved in 600 μL of MeOH and only 1/3 of the mixture was methylated. One third of F5 (200 μL) with methyl nonadecanoate ($C_{19:0}$, purity ≥98%, Sigma-Aldrich) as IS (8 mg/L) was dissolved in 5 mL MeOH and 400 μL sulfuric acid as catalyst was added. The tubes were capped and heated for 240 min at 70 °C in a RapidVap® Evaporator. Then, 10 mL of satured bicarbonate solution (2.125 g in 25 mL) to neutralize the reaction and 3 mL of hexane were added and the solution was gently stirred (1 min). This last solvent extraction was repeated three times. The upper phase containing the FAMEs was dried under a N_2 flow, redissolved with 10 μL of EtOAc and 40 μL of hexane and transferred into a gas chromatography (GC) vial. It is worth mentioning that the IS must be cautiously selected according to the particular kind of sample because $C_{19:0}$ may appear in soils and plant material and thus quantification using this molecule could be flawed. Nevertheless, previous studies analyzing fatty acids in plants and soils have used $C_{19:0}$ as the IS (Bühring et al., 2006; Sañé et al., 2011; Alewell et al., 2016; Đurovic et al., 2018) and some studies analyzing plant extracts of *Celtis* species (including *Celtis australis*) have not found this mentioned fatty acid (Santa-Cruz et al., 1975; Ihara and Tanaka, 1978; Semwal and Semwal, 2012). Here, we analyzed the three most concentrated samples (in fatty acids) among the different anatomical parts selected (leaves, bark and xylem) and $C_{19:0}$ was not detected.

The *n*-alkane, aromatic and fatty acid fractions were analyzed and quantified by gas chromatography equipped with a HP-5MS capillary column (30 m length × 0.25 mm i.d., 0.25 μm film thickness) coupled to a mass-selective detector (GC-Agilent 7890B, MSD Agilent 5977A) with an electron impact interface, at the Archaeological Micromorphology and Biomarker Research Laboratory (University of La Laguna, Spain). The GC was programmed to an initial temperature of 70 °C for 2 min, heated with a heating rate of 12 °C/min to 140 °C and to final temperature of 320 °C with a heating rate of 3 °C/min and held for 15 min, with helium as the carrier gas (2 mL/min). The total run time was 82.83 min to avoid overlap or interferences with other compounds (e.g., Jambrina-Enríquez et al., 2016). The multimode injector was held at a split ratio of 5:1 at an initial temperature of 70 °C during 0.85 min and heated to 300 °C at 720 °C/min. All measurements were repeated three times. The MS was operated in full scan mode (*m*/*z* 40–580) with an electron ionization energy of 70 eV and with the temperatures of the ion source and quadrupole set at 230 °C and 150 °C, respectively. Quantification was carried out taking the four most intense fragment ions (*m*/*z* 43, 57, 71 and 85, and *m*/*z* 67, 95, 81 and 245 for IS) for *n*-alkanes and the total ion chromatogram for the rest of the analytes.

Compounds were identified by comparison of their retention times and mass spectra with those of reference compounds (mix C_8–C_{40}, 500 mg/L of each *n*-alkane in DCM, purity ≥90.1%, Sigma-Aldrich) for F1 and 37 component FAME mix C_4–C_{24} (concentration in DCM varied from 200 to 600 mg/L, purity from 96.8 to 99.9%, Sigma-Aldrich), $C_{26:0}$ (purity ≥95%, Sigma-Aldrich), $C_{28:0}$ (purity ≥98%, Aldrich) and $C_{30:0}$ (purity ≥98%, Aldrich) for F5 and comparison with the NIST mass spectra library. Quantification was based on calibration curves obtained by plotting the area/$area_{IS}$ ratio versus the concentration of each reference compound. Correlation

coefficients were >0.995. We extracted all the fractions, but we focus on F1, F2 and F5 here. Since the standard for fatty acids is composed of FAMEs, the final quantitation for this class of compounds was made by multiplying the molecular weight factor (molar mass of fatty acid divided by the molar mass of FAME) by the mass of FAME obtained from calibration. The *n*-alkane, aromatic and fatty acid concentrations were normalized to sample weight (dry sample or charred sample) and expressed as μg of individual compound per gram of sample (μg/g sample) and normalized to mass of dry starting material (μg/g).

Mass loss was calculated as the percentage difference between the initial and the final weight, after dividing by the initial weight. A 0.1 mg precision digital scale (Entris®-Sartorius 224i.1S) was used for this weight measurement.

To evaluate the *n*-alkane distribution we calculated the CPI using the Bray and Evans equation (1961) (Eqs. (1) and (2)). In addition, we applied the CPI for fatty acids in which even-numbered fatty acids predominate over odd *n*-fatty acids (e.g., Knicker et al., 2013). For *n*-alkanes, we used the C_{25}–C_{33} interval (Eq. (1)) and for *n*-fatty acids the C_{14}–C_{30} range (Eq. (2)):

$$CPI_{25-33} = \left[\left(\sum C_{25-33odd} / \sum C_{24-32even}\right) + \left(\sum C_{25-33odd} / \sum C_{26-34even}\right)\right] \times 0.5 \quad (1)$$

$$CPI_{14-30} = \left[\left(\sum C_{14-30even} / \sum C_{13-29odd}\right) + \left(\sum C_{14-30even} / \sum C_{15-31odd}\right)\right] \times 0.5 \quad (2)$$

The ACL was calculated following the recommendation of Freeman and Pancost (2014) (Eqs. (3) and (4)); for total *n*-alkanes we used the C_{15}–C_{33} interval (Eq. (3)) and for odd-numbered *n*-alkanes we used the C_{25}–C_{33} interval (Eq. (4)):

$$ACL_{15-33total} = \sum (Ci \times [Ci]) / \sum [Ci]; 15 \leqslant i \leqslant 33 \quad (3)$$

$$ACL_{25-33odd} = \sum (Ci \times [Ci]) / \sum [Ci]; 25 \leqslant i \leqslant 33 \quad (4)$$

The value [Ci] is the concentration of the *n*-alkane with i carbon atoms.

2.4. Compound-specific carbon isotope analysis

Carbon isotope analyses of individual *n*-alkanes were made using a Thermo Scientific Isotope Ratio Mass Spectrometer Delta V Advantage coupled to a GC Trace1310 through a Conflo IV interface with a temperature converter GC Isolink II, at the Archaeological Micromorphology and Biomarker Research Laboratory (University of La Laguna, Spain). Samples were injected by means of a Programmed Temperature Vaporising injector (PTV) in splitless mode at an initial temperature of 60 °C (held 0.05 min), followed by an evaporation stage with the temperature increasing to 79 °C (held 0.5 min) and a transfer stage increasing to 325 °C (held 3 min), both of them with a rate of 10 °C/s. Finally, the cleaning temperature increased to 350 °C (held 3 min) at 14 °C/s. The GC was fitted with a Trace Gold 5-MS (Thermo Scientific) fused silica capillary column (30 m length × 0.25 mm i.d., 0.25 μm film thickness). Helium was used as the carrier gas at a flow rate set at 1.5 mL/min. The temperature programme comprised a 2 min isothermal period at 70 °C, followed by an increase in temperature to 140 °C at a rate of 12 °C/min and held for 2 min. Subsequently the temperature was increased to 320 °C at a rate of 3 °C/min and held for 15 min. The combustion reactor temperature was maintained at 1000 °C. Data acquisition and processing were carried out using the Isodat 3.0 software (Thermo Scientific). All measurements were repeated three times. $\delta^{13}C$ values were normalized to the Vienna Pee Dee Belemnite (VPDB) scale using a *n*-alkane Schimmelmann type A6 mixture (*n*-C_{16} to *n*-C_{30}) of known isotopic composition. The standard deviation of carbon isotope measurements was better than ±0.5‰.

3. Results and discussion

3.1. Fresh plant wax n-alkyl components: Celtis australis anatomical part characterization

As expected for a woody sample with a low contribution of epicuticular waxes to sediments (Diefendorf and Freimuth, 2017), the total concentration of *n*-alkanes in fresh *Celtis* wood (branches and twigs) was lower (19.4 and 8.6 μg/g sample) than in fresh *Celtis* leaves (459.1 μg/g sample) and more abundant in the bark (7.7–18.5 μg/g sample) than in the xylem samples (~0.9 μg/g sample) (Table 1). Similar findings were found among leaves and stems from herbs, grasses and shrubs (Gocke et al., 2011; Gamarra and Kahmen, 2015) and among leaves and branches from trees (Adams and Wright, 2012). In addition to the significant difference in concentrations of *n*-alkanes, the leaf, branch and twig samples showed different *n*-alkane distribution patterns. Long-chain *n*-alkanes with a predominance of odd numbered *n*-alkane (maximizing at C_{31}) were dominant in *Celtis australis* leaf samples (Table 1). This distribution pattern is typical for higher plants containing long chain *n*-alkanes (*n*-C_{27}, *n*-C_{29} and *n*-C_{31}) in their epicuticular waxes (Eglinton and Hamilton, 1967) and has been described in other species of *Celtis* trees such as *Celtis occidentalis* (*n*-C_{29} n = 1; Diefendorf et al., 2011; Bush and McInerney, 2015; Diefendorf and Freimuth, 2017) and *Celtis laevigata* (*n*-C_{29} n = 1 and *n*-C_{31} n = 3, Bush and McInerney, 2015; Diefendorf and Freimuth, 2017).

The woody samples (twigs and branches) displayed different *n*-alkane distribution patterns. Fresh *C. australis* twigs (bark and xylem samples) were dominated by long carbon chain lengths (*n*-C_{29} max) while branches (bark and xylem) showed higher amounts of mid-chain *n*-alkanes (*n*-C_{25} max) and a lower long-chain *n*-alkane content (Table 1). Similarly, higher concentrations of mid-chain *n*-alkanes have been reported in tree-wood samples (e.g., *Quercus nigra*, O'Malley et al., 1997 and *Pinus sylvestris*, Knicker et al., 2013) and higher amounts of long-chain *n*-alkanes in herb-stems and shrub-stems (e.g., rye, wheat and maize: Wiesenberg et al., 2004; *Robinia pseudoacacia* and *Solidago canadensis* L.: Gocke et al., 2011).

It is well known that mid-chain *n*-alkanes (such as *n*-C_{23} or *n*-C_{25}) in sediments are mainly derived from submerged/floating aquatic plants (Ficken et al., 2000) and from terrestrial higher plants to a lesser extent (Jansen et al., 2006), whereas long-chain *n*-alkanes (such as *n*-C_{27}, *n*-C_{29} or *n*-C_{31}) are mainly derived from terrestrial plants (Eglinton and Hamilton, 1967). Based on this observation, the terrestrial/aquatic plant ratio (Paq, Ficken et al., 2000) has been widely applied to identify aquatic and terrestrial plant inputs and paleohydrological changes in lacustrine sediments (Meyers, 2003). However, according to our results and previous findings, the abundance of mid-chain *n*-alkanes (*n*-C_{21}, *n*-C_{23}, *n*-C_{25}) in wood (i.e. branches or wood cores from trees) should be considered, particularly in contexts involving combustion structures fuelled by wood.

Some indexes such as ACL and CPI of *n*-alkanes are used as indicators of the source and degree of OM diagenesis (Cranwell, 1973; Meyers, 2003). However, it has been suggested that there are no significant differences between the ACL values of vegetation types (woody and non-woody plants) and that climate may influence ACL values (Bush and McInerney, 2015; Wang et al., 2015). In

Table 1
Quantitative results of *n*-alkanes and fatty acids in fresh and charred leaves, branches and twigs. Total alkanes and total fatty concentrations normalized to sample weight (μg per gram of sample, μg/g sample), alkane and fatty acid ranges (Crange), most abundant *n*-alkane and *n*-fatty acid (Cmax), average chain length ($ACL_{15-33total}$ and $ACL_{25-33odd}$) for *n*-alkanes, carbon preference index (CPI) for *n*-alkanes (CPI_{25-33}) and for *n*-fatty acids (CPI_{14-30}). Mass loss (%) and total alkanes and fatty acid concentrations normalized to mass of dry starting material (μg/g).

	Celtis leaves REF	*Celtis* leaves 150 °C 1 h	*Celtis* leaves 250 °C 1 h	*Celtis* leaves 250 °C 3 h	*Celtis* leaves 250 °C 5 h	*Celtis* leaves 350 °C 1 h	*Celtis* leaves 450 °C 1 h
Total alkanes (μg/g sample)	459.1	484.0	360.6	335.9	177.3	97.0	28.8
Crange	C_{21}-C_{33}	C_{21}-C_{33}	C_{18}-C_{33}	C_{19}-C_{33}	C_{19}-C_{33}	C_{19}-C_{33}	C_{19}-C_{33}
Cmax	C_{31}	C_{31}	C_{31}	C_{31}	C_{31}	C_{31}	C_{31}
CPI_{25-33}	2.7	3.3	5.6	4.0	6.3	4.3	1.1
$ACL_{15-33total}$	30.3	30.4	30.3	30.2	30.0	28.1	28.7
$ACL_{25-33odd}$	30.3	30.4	30.5	30.4	30.3	30.1	29.7
Total FA (μg/g sample)	8.9	68.1	24.7	13.1	21.4	35.1	_
Crange	$C_{14:0}$-$C_{22:0}$	$C_{14:0}$-$C_{24:0}$	$C_{16:0}$-$C_{26:0}$	$C_{16:0}$-$C_{26:0}$	$C_{16:0}$-$C_{22:0}$	$C_{14:0}$-$C_{26:0}$	_
Cmax	$C_{18:0}$	$C_{18:2}$	$C_{26:0}$	$C_{26:0}$	$C_{16:0}$	$C_{16:0.\ C26:0}$	_
CPI_{14-30}	4.7	3.8	4.0	5.9	5.8	6.7	_
Mass loss (%)		17	35	39	52	56	74
Total alkane (μg/g)	459.1	585.3	558.3	548.8	366.2	221.9	119.1
Total FA (μg/g)	8.9	82.4	38.3	21.3	44.2	93.8	_

	Celtis bark branches REF	*Celtis* bark branches 150 °C 1 h	*Celtis* bark branches 250 °C 1 h	*Celtis* bark branches 350 °C 1 h	*Celtis* bark branches 450 °C 1 h
Total alkanes (μg/g sample)	18.5	4.2	3.5	8.5	0.1
Crange	C_{16}-C_{30}	C_{19}-C_{31}	C_{16}-C_{29}	C_{16}-C_{30}	C_{20}-C_{24}
Cmax	C_{25}	C_{25}	C_{22}	C_{21}-C_{22}	*
CPI_{25-33}	3.1	3.4	1.6	1.1	_
$ACL_{15-33total}$	23.9	25.1	23.4	22.9	21.9
$ACL_{25-33odd}$	26.5	26.9	27.9	26.6	_
Total FA (μg/g sample)	60.0	36.5	8.8	11.3	_
Crange	$C_{14:0}$-$C_{30:0}$	$C_{14:0}$-$C_{28:0}$	$C_{16:0}$-$C_{28:0}$	$C_{16:0}$-$C_{30:0}$	_
Cmax	$C_{18:2}$	$C_{18:2}$	$C_{26:0}$	$C_{30:0}$	_
CPI_{14-30}	10.7	9.8	14.6	15.9	_
Mass loss (%)		14	32	54	76
Total alkane (μg/g)	18.5	4.8	5.2	18.5	0.2
Total FA (μg/g)	60.0	42.5	13.1	24.7	_

	Celtis xylem branches REF	*Celtis* xylem branches 150 °C-1 h	*Celtis* xylem branches 250 °C-1 h	*Celtis* xylem branches 350 °C-1 h	*Celtis* xylem branches 450 °C-1 h
Total alkane (μg/g sample)	0.9	0.9	1.2	1.6	0.1
Crange	C_{18}-C_{29}	C_{16}-C_{29}	C_{16}-C_{29}	C_{16}-C_{27}	C_{20}-C_{25}
Cmax	C_{25}	C_{25}	C_{22}	C_{21}-C_{22}	*
CPI_{25-33}	1.3	1.3	1.3	1.5	_
$ACL_{15-33total}$	24.3	24.0	23.2	21.8	22.7
$ACL_{25-33odd}$	26.9	26.9	27.1	26.0	25.0
Total FA (μg/g sample)	32.1	47.4	10.7	0.3	_
Crange	$C_{16:0}$-$C_{18:0}$	$C_{16:0}$-$C_{18:0}$	$C_{16:0}$-$C_{18:0}$	$C_{16:0}$-$C_{18:0}$	_
Cmax	$C_{18:2}$	$C_{18:2}$	C_{16}	$C_{18:1}$	_
CPI_{14-30}	_	_	_	_	_
Mass loss (%)		18	37	64	76
Total alkanes (μg/g)	0.9	1.1	2.0	4.5	0.2
Total FA (μg/g)	32.1	58.0	17.1	0.8	_

	Celtis bark twigs REF	*Celtis* bark twigs 150 °C-1 h	*Celtis* bark twigs 250 °C-1 h	*Celtis* bark twigs 350 °C-1 h	*Celtis* bark twigs 450 °C-1 h
Total alkane (μg/g sample)	7.7	3.2	4.5	7.3	0.1
Crange	C_{19}-C_{31}	C_{21}-C_{31}	C_{16}-C_{30}		
Cmax	C_{29}	C_{29}	*	*	*
CPI_{25-33}	2.8	4.1	1.2	1.3	0.8
$ACL_{15-33total}$	25.9	27.4	25.1	22.3	24.2
$ACL_{25-33odd}$	27.7	28.2	27.4	26.8	26.0
Total FA (μg/g sample)	9.0	33.7	4.8	5.3	_
Crange	$C_{16:0}$-$C_{22:0}$	$C_{16:0}$-$C_{22:0}$	$C_{16:0}$-$C_{22:0}$	$C_{16:0}$-$C_{22:0}$	_
Cmax	$C_{18:2}$	C_{22}	$C_{18:2}$	C_{22}	_
CPI_{14-30}	23.4	14.0	5.0	2.9	_
Mass loss (%)		6	25	55	66
Total alkanes (μg/g)	7.7	3.4	6.0	16.0	0.3
Total FA (μg/g)	9.0	35.7	6.4	11.9	_

(*continued on next page*)

Table 1 (*continued*)

	Celtis xylem twigs REF	*Celtis* xylem twigs 150 °C-1 h	*Celtis* xylem twigs 250 °C-1 h	*Celtis* xylem twigs 350 °C-1 h	*Celtis* xylem twigs 450 °C-1 h
Total alkane (μg/g sample)	0.9	0.8	0.2	0.4	0.1
Crange	C_{16}-C_{29}	C_{17}-C_{29}	C_{17}-C_{29}	C_{16}-C_{29}	C_{20}-C_{24}
Cmax	C_{29}	C_{29}	*	*	*
CPI_{25-33}	1.2	1.3	1.3	1.8	_
$ACL_{15-33total}$	26.4	25.7	23.6	22.9	22.6
$ACL_{25-33odd}$	28.9	28.0	27.0	27.0	26.0
Total FA (μg/g sample)	8.6	62.1	22.3	0.4	_
Crange	$C_{16:0}$-$C_{22:0}$	$C_{16:0}$-$C_{23:0}$	$C_{16:0}$-$C_{23:0}$	$C_{16:0}$-$C_{23:0}$	_
Cmax	$C_{18:2}$	C_{16}	C_{16}	$C_{18:2}$	_
CPI_{14-30}	_	10.5	4.7	0.9	_
Mass loss (%)		7	30	66	73
Total alkanes (μg/g)	0.9	0.8	0.3	1.1	0.3
Total FA (μg/g)	8.6	63.4	31.9	1.2	_

$CPI_{25-33} = [(\Sigma C_{25-33odd}/\Sigma C_{24-32even}) + (\Sigma C_{25-33odd}/\Sigma C_{26-34even})] \times 0.5$.
$CPI_{14-30} = [(\Sigma C_{14-30even}/\Sigma C_{13-29odd}) + (\Sigma C_{14-30even}/\Sigma C_{15-31odd})] \times 0.5$.
$ACL_{15-33total} = \Sigma\ (Ci \times [Ci])/\Sigma\ [Ci];\ 15 \leq i \leq 33$.
$ACL_{25-33odd} = \Sigma\ (Ci \times [Ci])/\Sigma\ [Ci];\ 25 \leq i \leq 33$.
_: No data.
*: No Cmax.

our study, the highest ACL_{15-33} values were recorded in leaf samples (ACL = 30.3). ACL_{15-33} values in branch samples (bark = 23.9 and xylem = 24.3) were lower than in twig samples (bark = 25.9 and xylem = 26.4) (Table 1). Similarly, the highest ACL_{25-33} were found in leaf (ACL = 30.3) and twig (ACL ≈ 28) samples. The low abundance of long-chain *n*-alkanes in branch samples caused low ACL_{25-33} (ACL < 27) (Table 1). We found that the ACL values in *C. australis* leaf samples were within the *C. occidentalis* and *C. laevigata* ACL range (Diefendorf and Freimuth, 2017). Higher ACL values (ACL = 28–30) were reported in leaves and stems of grasses, herbs and shrubs (Gocke et al., 2011; Gamarra and Kahmen, 2015) and lower ACL values (ACL ≈ 22) in pine wood (Knicker et al., 2013).

It is well established that *n*-alkanes derived from terrestrial plants are characterized by long chain homologues with a high odd over even predominance (CPI = 5–10; Eglinton and Hamilton, 1967; Rieley et al., 1991; Eglinton and Hamilton, 1967; Rieley et al., 1991), whereas CPI values close to one are thought to indicate highly degraded OM (Cranwell, 1981). Fresh *C. australis* leaf samples had low CPI_{25-33} values (CPI = 2.7) similar to those calculated for *C. occidentalis* leaves by Diefendorf et al. (2011).

There are about 70 different *Celtis* species distributed in the temperate and tropical areas. *C. laevigata* (Mississippi hackberry or sugarberry) prevails in the more humid soils in central North America whereas in eastern North America *C. occidentalis* (hackberry or nettle tree) is dominant (Demır et al., 2002). In the Mediterranean region, *C. australis* (Mediterranean hackberry or European nettle tree) can be found in dry rocky settings or in deep moist alluvial soils (Costa et al., 1998). The lower CPI_{25-33} values in xylem samples (CPI = 1.2–1.3) compared to those that correspond to the bark samples (CPI = 2.8–3.1) could be due to a low abundance of epicuticular waxes (Table 1). CPI values ~ 2 were recorded for tree wood samples (O'Malley et al., 1997; Knicker et al., 2013), whereas CPI of stems (herbs and shrubs) samples varied from 2 to 19 (Gocke et al., 2011).

In addition to straight chain *n*-alkanes, a series of *n*-alkenes ranging from *n*-$C_{20:1}$ to *n*-$C_{25:1}$ was identified in the bark of the branch samples, with a terminal double bond, an even-over-odd dominance in the carbon number and C_{max} at *n*-$C_{20:1}$. These compounds eluted just before the corresponding *n*-alkanes and their concentrations were lower than those of the corresponding *n*-alkanes. Although *n*-alkenes are not major components in plant waxes, long-chain *n*-alkenes ranging from *n*-$C_{21:1}$ to *n*-$C_{27:1}$ with an odd (Duan and Ma, 2001; Pu et al., 2017) or even carbon predominance (Pu et al., 2017) have been ascribed to epicuticular waxes of terrestrial plants.

The fatty acid fraction consisted mainly of satured as well as mono and di-unsatured straight-chain homologues. The total concentration of fatty acids in fresh *Celtis* branches (bark and xylem, 60.0 and 32.1 μg/g sample respectively) was higher than in fresh *Celtis* leaf and twig (bark and xylem) samples (~9 μg/g sample) and higher than those obtained for alkanes (Table 1). Similarly, higher concentrations of fatty acids than *n*-alkanes were reported in pine wood (Knicker et al., 2013). Leaf samples contained high proportions of even-numbered mid-chain acids (between *n*-C_{14} and *n*-C_{22}) with stearic acid (*n*-$C_{18:0}$) as dominant. The long-chain fatty acids were present in minor amounts. This distribution pattern is typical for higher plants (Eglinton and Hamilton, 1967).

It has been reported that high-molecular-weight fatty acids ($\geq C_{20}$) in sediments are derived from terrestrial higher plants, whereas low-molecular-weight fatty acids ($\leq C_{19}$) have multiple sources such as vascular plants, microbes and marine phytoplankton (Simoneit and Mazurek, 1982; Fine et al., 2001; Kawamura et al., 2003; Fu et al., 2013). Moreover, $C_{16:0}$, $C_{18:2}$, $C_{18:1}$, $C_{18:0}$ are the main compounds produced during lipid biosynthesis (e.g., Bianchi, 1994). The fatty acid distribution in branches (bark and xylem) and twigs (bark and xylem) was dominated by mid-chain acids ranging from *n*-C_{14} to *n*-C_{30}, with higher values of octadecadienoic isomer mixture (*n*-$C_{18:2}$). Long-chain acids were present in minor amounts with a dominance of even carbon numbers (*n*-C_{26}, *n*-C_{28} and *n*-C_{30}) (Table 1). This fatty acid distribution has been observed in stems of C3 plants (Wiesenberg et al., 2004). In contrast to the alkanes, the saturated fatty acid of leaves, branches and twigs (bark) were characterized by an even-to-odd carbon number predominance with a CPI_{14-30} of 4.7 (leaves), 10.7 (bark-branches) and 23.4 (bark twigs).

3.2. Molecular changes in charred biomass: aliphatic and aromatic hydrocarbons and fatty acids

In the first stage of thermal alteration (150 °C) the leaf and branch samples lost 17% and 14–18% of mass respectively, whereas the mass loss of twig samples was 6–7% (Table 1). The *n*-alkane distribution pattern in leaf and woody samples (branches and twigs) after 1 h of burning at 150 °C was similar to the unheated samples with *n*-C_{31} as the dominant alkane in leaf samples, *n*-C_{25} in branch samples (bark and xylem) and *n*-C_{29} in twig samples (bark and xylem) (Fig. 1). The fatty acid *n*-$C_{18:2}$ was abundant in all the samples, although *n*-$C_{16:0}$ and *n*-$C_{22:0}$ were higher in twig samples (Fig. 2). At this temperature, the *n*-alkane concentration

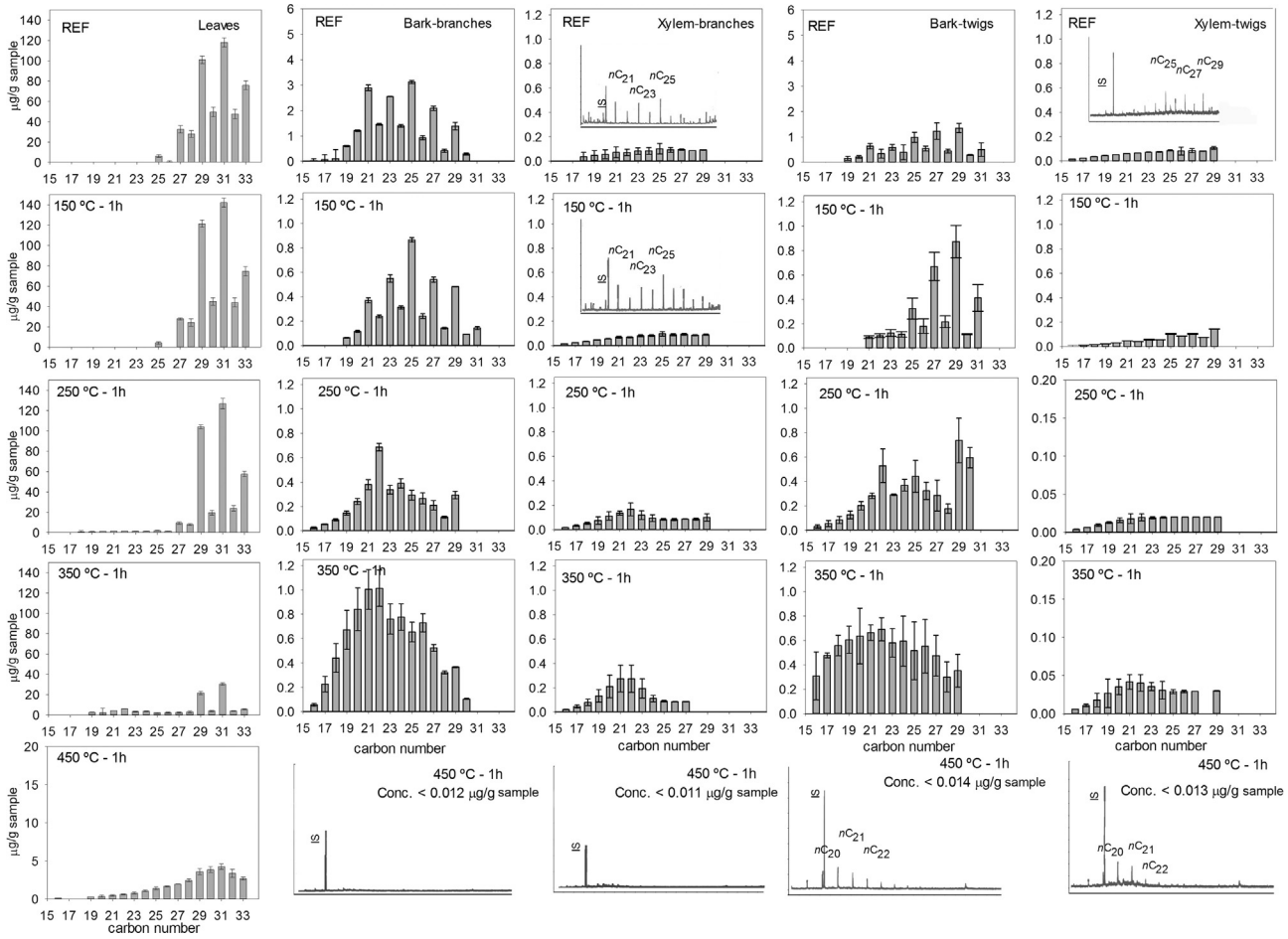

Fig. 1. Histograms showing the distributions and abundance of *n*-alkanes in fresh and charred leaves, branches (bark and xylem) and twigs (bark and xylem) with the associated error value (n = 3, α = 0.05). IS: 5α-androstane. The concentrations (Conc.) are given in µg per g of (dry or charred) sample (µg/g sample).

in the leaf samples was higher than in the starting composition (Fig. 3) which is consistent with other studies (Diefendorf et al., 2015), whereas for the bark samples the *n*-alkane and *n*-alkene (Cmax at n-$C_{24:1}$) concentrations decreased. The ACL in leaf and bark samples remained in the higher value range (ACL_{leaves} = 30.4; $ACL_{15–33\text{-}bark}$ ranged from 25.1 to 27.4 and $ACL_{25–33\text{-}bark}$ ranged from 26.9 to 28.2) supporting the observed low alteration of *n*-alkane composition at low temperatures (Fig. 3). The $CPI_{alkanes}$ values increased ($CPI_{25–33\text{-}leaves}$ = 3.3 and $CPI_{25–33\text{-}bark}$ ranged from 3.4 to 4.1) whereas the $CPI_{fatty\text{-}acid}$ values decreased ($CPI_{14–30\text{-}leaves}$ = 3.8 and $CPI_{14–30\text{-}bark}$ ranged from 9.8 to 14.0).

The fatty acid concentration generally exceeded that from the unheated samples except for bark-branch samples, for which there was a decrease in fatty acid content (Fig. 3). The xylem samples contained lower *n*-alkane and higher *n*-fatty acid concentrations than in the starting composition. The ACL_{xylem} decreased ($ACL_{15–33}$ = 24.0–25.7 and $ACL_{25–33}$ = 26.9–28.0) and no significant alteration was recorded in CPI_{xylem} ($CPI_{25–33}$ = 1.3) by charring (Fig. 3). In fact, PAHs originating from incomplete burning of organic matter (Yunker et al., 2002) were not present in detectable amounts at this temperature. However, we found two degradation products: One, neophytadiene, (7,11,15-trimethyl-3-methylene-1-hexadecene), a phytadiene isomer (terpene), is a degradation product of chlorophyll (Rowland, 1957; Venkata et al., 2012; Abdel-Aal et al., 2015) and was detected in the leaf samples. The other, stigmasta-3,5-diene, a degradation product of phytosterols (Cert et al., 1994) was identified in branch and twig samples. Braadbaart and Poole (2008) conducted a series of experiments using pine and oak wood to produce charcoal at temperatures from 160 to 1200 °C with an exposure time of 2–1440 min. Their results show that at 160 °C the molecular composition (polysaccharides and lignin markers) of heated *Pinus* and *Quercus* wood samples was similar to unheated wood.

As temperature increased, the mass loss in all the samples was around 25–37% (Table 1). At 250 °C, the charred anatomical parts of *C. australis* revealed different features. The leaf samples showed similar *n*-alkane distribution to the unheated samples (*n*-Cmax at 31 and a predominance of the odd carbon numbered chains) (Fig. 1), higher *n*-alkane concentration, high ACL ($ACL_{15–33}$ = 30.3 and $ACL_{25–33}$ = 30.5) and CPI_{alkane} ($CPI_{25–33}$ = 5.6) values and low $CP_{fatty\text{-}acid}$ ($CPI_{14–30}$ = 24.7) which is consistent with other studies (Diefendorf et al., 2015) and indicative of an immature stage of thermal alteration (Fig. 3) However, the alkane series from the woody samples tended to show a pattern typical of thermal degradation: higher content of low molecular weight alkanes with an even-carbon number preference (the maximum was found in the n-C_{20}–n-C_{22} range), lower *n*-alkane (*n*-Cmax at 22) and *n*-alkene concentrations (*n*-Cmax at 24). The ACL and the CPI in bark and xylem samples decreased ($ACL_{15–33\text{-}branches} \approx 23$, $ACL_{15–33\text{-}twigs}$ = 23.6–25.1; $CPI_{25–33\text{-}branches}$ = 1.3–1.6, $CPI_{25–33\text{-}twigs}$ = 1.2–1.3 (Figs. 1 and 3).

Although the fatty acid concentrations decreased in the leaf and woody samples, fatty acid patterns were quite resistant to heat (with maxima at n-$C_{16:0}$, n-$C_{18:2}$ or n-$C_{26:0}$) (Figs. 2 and 3) with $CPI_{14–30}$ values ranging from 4.0–5.0 (leaves and twigs) to 14.6 (branches). Besides the chain breakdown suggestive of thermal

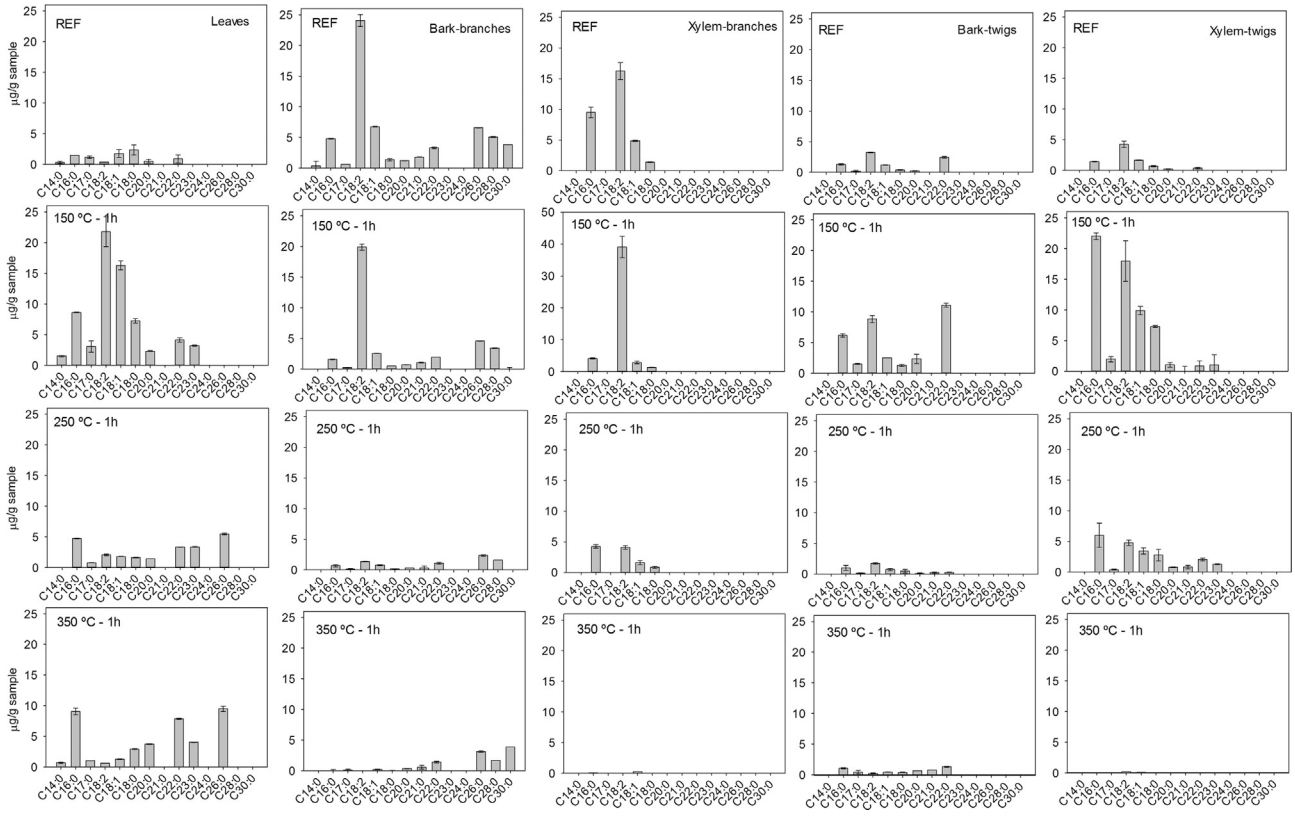

Fig. 2. Distribution and abundance of individual fatty acids in fresh and charred leaves, branches (bark and xylem) and twigs (bark and xylem) with the associated error value (n = 3, α = 0.05). The concentrations (Conc.) are given in µg per g of (dry or charred) sample (µg/g sample).

transformation, PAHs were not present in detectable amounts at this temperature; only dimethylnaphthalene, which consists of two coplanar fused rings, was found in the leaf samples at low concentrations (0.04 µg/g sample) and some phytosterol degradation products (stigmasta-3,5-diene) in branch and twig samples. The findings of Braadbaart and Poole (2008) suggest that main molecular constituents of wood (i.e. cellulose, hemicellulose and lignin) begin to transform into aromatic compounds at a temperature of 280 °C.

Since average temperatures associated with black sedimentary layers are below 300 °C (Mallol et al., 2013) and the molecular composition of leaf samples was not found to be affected by progressive heating, we decided to explore the influence of combustion duration by heating the samples to 250 °C for a scheduled period of 3 and 5 h. During the first and third hour of charring, the leaf samples lost 35% and 39% of mass respectively. After 5 h these percentages increased to 52%. With increasing time of charring (3 and 5 h) the *n*-alkane distribution patterns were similar to the samples heated at 250 °C during 1 h (maximum at n-C_{31} and a predominance of the odd-carbon numbered chains) (Table 1 and Fig. 4). The *n*-alkane concentrations decreased with increasing burning time (Fig. 4). After 5 h of combustion, the ACL_{leaves} ratios reached the lowest values ($ACL_{15–33}$ = 30.0) and the $CPI_{25–35\text{-leaves}}$ (6.3) and $CPI_{14–30}$ (5.8) ratios the highest values (Fig. 4). The concentrations of total fatty acids and the abundance of n-$C_{16:0}$ decreased after 3 h of charring followed by an increase in both after 5 h (Fig. 4). Simple aromatic compounds (methyldecyl)-benzene, (dimethyldecyl)-benzene, (hexadecyl)-benzene, (methylhexadecyl)-benzene and naphthalene were identified after 3 and 5 h of combustion. More complex PAHs (methylanthracene and trimethylphenanthrene), which both contain three fused aromatic rings, were found after 5 h of combustion. Similar findings were reported by heating rye and maize at 300 °C under oxygen-limited conditions (Wiedemeier et al., 2015).

A further increase in combustion temperature to 350 °C resulted in an increased in the percentage of mass loss to 54–66% (Table 1). With heating, the leaf samples recorded a shortening of the *n*-alkane chain length and a small increase of mid-chain homologues, but with a predominance of odd numbered alkanes (n-C_{31}) (Fig. 1). The total *n*-alkane concentration decreased from 558 to 222 (concentration loss around 60%), the $ACL_{15–33\text{-leaves}}$ value dropped from 30.3 to 28.1 and the $ACL_{25–33\text{-leaves}}$ from 30.5 to 30.1), but the CPI_{leaves} ratio remained higher ($CPI_{25–33}$ = 4.3), consistent with the good state of the original *n*-alkane distribution pattern (Fig. 3). However, heat severely affected the woody samples (branches and twigs) as is recorded by the even numbered alkane chain length distribution centred around n-C_{20} to n-C_{22} (Fig. 1) and low ACL and CPI values ($ACL_{15–33}$ varies between 21.8 and 22.9, $ACL_{25–33}$ varies between 26.0 and 27.0 and $CPI_{25–33}$ varies between 1.1 and 1.8).

As identified in laboratory experiments by Knicker et al. (2013), the charring of wood (pine) at 350 °C (oxic conditions) can induce the thermal breakdown of long chain *n*-alkanes, the dominance of even homologues and the decrease in molecular CPI ratio. Whereas the concentration of *n*-alkanes in leaf samples decreased, in woody samples, and more evident in bark samples, it increased, which could result from breakdown processes of other higher molecular weight constituents of bark samples at higher temperatures (Fig. 3). The *n*-alkene concentration in the bark samples increased and tended to show a maximum at n-$C_{26:1}$, probably produced by hydrocarbon cracking or derived from dehydration of *n*-alkanols during incomplete combustion (Simoneit, 2002). Among fatty acids the concentration dropped to 0.8 in xylem samples whereas in leaf and bark samples the values increased ($CPI_{14–30}$ values varied

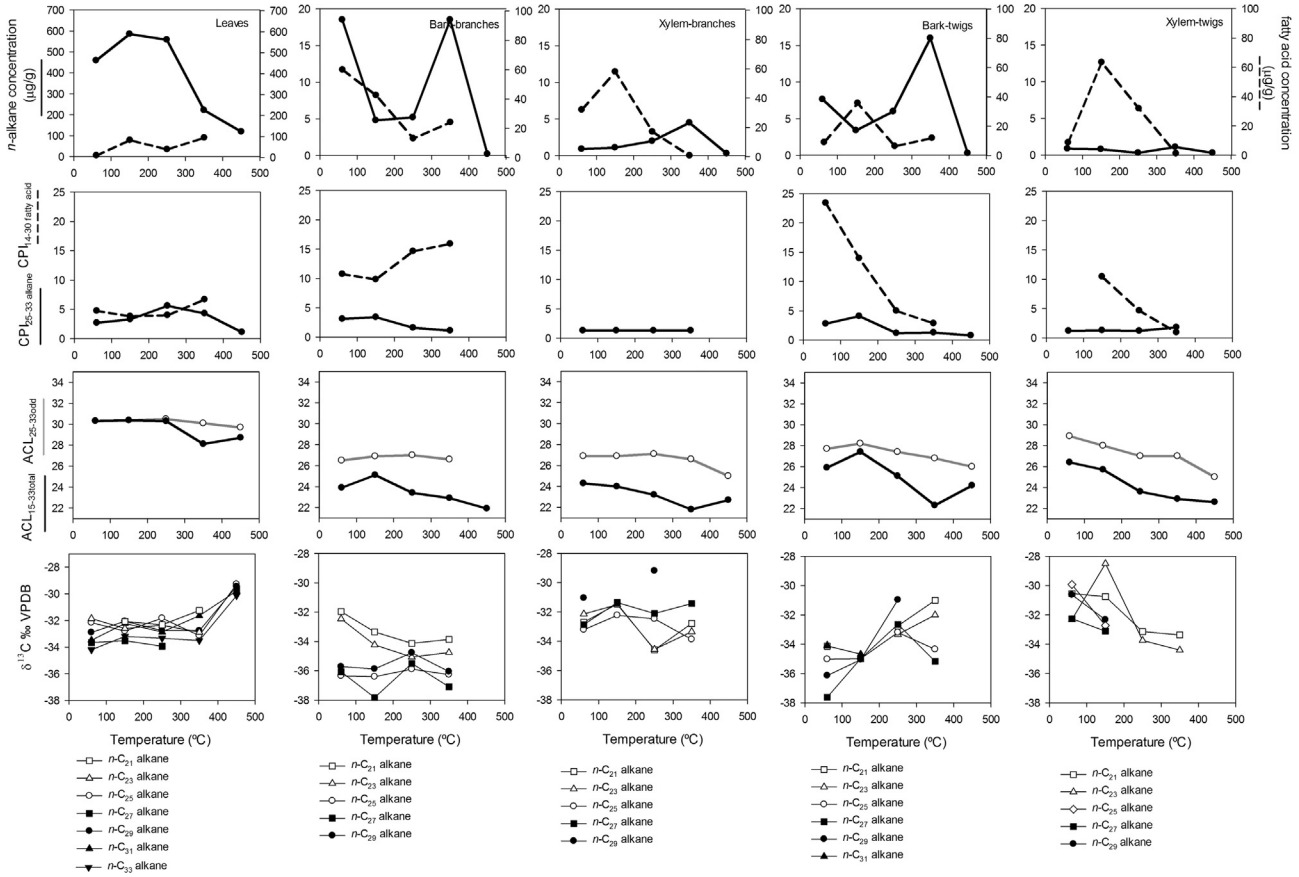

Fig. 3. Variation in *n*-alkane and fatty acid concentrations (normalized to mass of dry starting material, µg/g), $CPI_{25–33}$, $ACL_{15–33total}$ and $ACL_{25–33odd}$ values of *n*-alkanes, $CPI_{14–30}$ values of fatty acids and $\delta^{13}C_{alkane}$ for fresh and charred samples. Unaltered samples are plotted at 60 °C. $CPI_{25–33} = [(\Sigma C_{25–33odd}/\Sigma C_{24–32even}) + (\Sigma C_{25–33odd}/\Sigma C_{26–34even})] \times 0.5$. $CPI_{14–30} = [(\Sigma C_{14–30even}/\Sigma C_{13–29odd}) + (\Sigma C_{14–30even}/\Sigma C_{15–31odd})] \times 0.5$. $ACL_{15–33total} = \Sigma(Ci \times [Ci])/\Sigma[Ci]$; $15 \leq i \leq 33$. $ACL_{25–33odd} = \Sigma(Ci \times [Ci])/\Sigma[Ci]$; $25 \leq i \leq 33$.

between 6.7 and 15.9) (Fig. 3). However, fatty acid series were highly responsive to heat, changing to a pattern with higher amounts of higher molecular weight acids (*n*-C_{26}, *n*-C_{28}, *n*-C_{30}) (Fig. 2).

Thermal degradation at 350 °C with limited oxygen conditions during incomplete biomass burning resulted in a different suite of PAHs between leaf and bark samples. Aromatics in xylem samples were below the limit of detection. The dominant aromatics in leaf samples were dimethyl-, trimethyl- and tetramethylnaphthalenes, anthracene, phenanthrene and methyldecyl-benzene in amounts ≤0.3 µg/g sample. Similar findings have been reported by Wiedemeier et al. (2015), studying 3-ring PAHs in char (maize and rye) produced at 300 °C. Bark samples were characterized by a series of C_{13}–C_{18} alkyl benzenes and a mixture of *n*-alkylmethylbenzenes and phenanthrene in amounts ≤0.03 µg/g sample. *n*-Alkyl benzenes are present in pyrolysis products (de La Rosa and Knicker, 2011) and are generated by the thermal degradation of lignin-derived structures at temperatures between 310 and 400 °C (Braadbaart and Poole, 2008).

At a charring temperature of 450 °C, all the samples lost 66–76% of their mass (Table 1). The leaf samples recorded the most drastic changes in *n*-alkane composition with an equal distribution of odd and even *n*-alkanes centered around *n*-C_{30} to *n*-C_{32} (Fig. 1). The *n*-alkane concentrations in wood samples was close to zero and the fatty acid concentration of leaves and wood were below the limit of detection (Fig. 3). With increasing temperature, the *n*-alkane concentration and ACL and CPI ratios decreased due to successive thermal degradation of biomass with values close to those of the 400 °C burning experiments reported by Wiesenberg et al. (2009). Although the $CPI_{25–33}$ values in leaf and woody samples were close to 1, the lowest $ACL_{15–33}$ was recorded in woody samples ($ACL_{15–33\text{-leaves}} = 28.7$, $ACL_{15–33\text{-branches}} = 21.9–22.7$, $ACL_{15–33\text{-twigs}} = 22.6–24.2$) (Fig. 3). At this temperature aromatic compounds were no longer observed.

3.3. n-Alkane stable carbon isotope composition: The effect of thermal degradation on different anatomical parts

Carbon isotope analyses of long-chain *n*-alkanes have proven useful to characterize past changes in vegetation (i.e. identifying the contribution of plants with C3 and C4 photosynthetic pathway to sediments) and as complements of the $\delta^{13}C$ values of bulk OM (Meyers, 2003). The stable carbon isotopic compositions of *n*-C_{27}–*n*-C_{31} odd *n*-alkanes in fresh *C. australis* leaves (Table 2) were consistently in the range of those of leaf wax *n*-alkanes in C3 vegetation (Diefendorf and Freimuth, 2017). Although no fresh leaves were collected in the winter season because *C. australis* is a deciduous tree, we have found compound-specific isotope variations between leaves (collected at 2 m above the ground) and branches-twigs. Branches (average $\delta^{13}C = -33.9‰$) and twigs (average $\delta^{13}C = -33.7‰$) were depleted by 0.7‰ and 0.5‰ relative to leaves. The xylem was enriched by ~2‰ in ^{13}C relative to leaves, whereas bark was depleted by ~3‰ in ^{13}C relative to leaves (Table 2). While the stable carbon isotopic compositions of *n*-C_{21}–*n*-C_{25} odd *n*-alkanes in fresh leaves was enriched in ^{13}C (average –32.0‰), those from branches and twigs were depleted

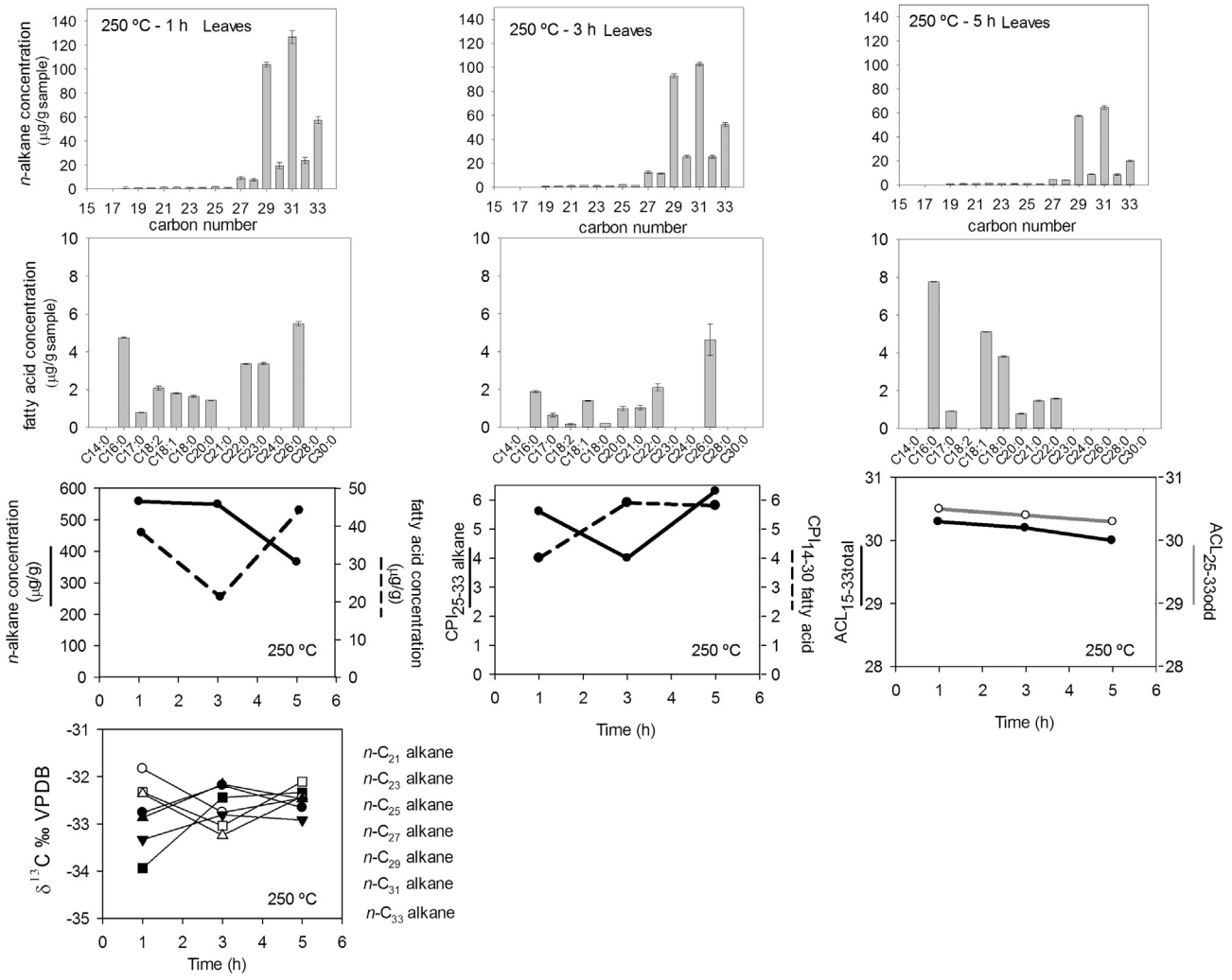

Fig. 4. *n*-Alkane distribution in leaves (µg per g of charred sample, µg/g sample) and variation in concentration (normalized to mass of dry starting material, µg/g), CPI_{25-33}, $ACL_{15-33total}$ and $ACL_{25-33odd}$ values of *n*-alkanes, CPI_{14-30} values of fatty acids and $\delta^{13}C_{alkane}$ generated at 250 °C during 1, 3 and 5 h. Unaltered samples are plotted at 60 °C. $CPI_{25-33} = [(\Sigma C_{25-33odd}/\Sigma C_{24-32even}) + (\Sigma C_{25-33odd}/\Sigma C_{26-34even})] \times 0.5$. $CPI_{14-30} = [(\Sigma C_{14-30even}/\Sigma C_{13-29odd}) + (\Sigma C_{14-30even}/\Sigma C_{15-31odd})] \times 0.5$. $ACL_{15-33total} = \Sigma(Ci \times [Ci])/\Sigma[Ci]$; $15 \leq i \leq 33$. $ACL_{25-33odd} = \Sigma\ (Ci \times [Ci])/\Sigma[Ci]$; $25 \leq i \leq 33$.

(average bark –33.6‰ and –34.4‰ respectively; average xylem: –32.7‰ and –30.9‰) (Table 2 and Fig. 3). Since leaves and wood differ in their chemical composition (e.g., lipids, lignin, cellulose, hemicellulose, sucrose) $\delta^{13}C_{bulk}$ values of these parts can differ by 2–3‰ (Ascough et al., 2008). The ^{13}C depletion of bulk wood compared to leaves can mainly be explained by its higher lignin content (depleted in ^{13}C) and lower cellulose content (enriched in ^{13}C) (Ehleringer et al., 2000). In fact, cuticular wax composition varies widely by tissue, organ or across stages of development within an individual organism (Post-Beittenmiller, 1996). In comparison to our analyses, Wiesenberg et al. (2004) found compound-specific isotope variations in long-chain alkanes for different parts of C3 and C4 plants. In C3 plants, stems were enriched by 1.4‰ in ^{13}C (rye grass) relative to leaves or with equal isotope value (wheat grass) whereas in C4 plants (maize) the *n*-alkanes from fresh stems were depleted in ^{13}C relative to leaves (Wiesenberg et al., 2004). These isotope variations between different plant parts has been explained as a result of internal biosynthetic fractionation during C transport and fixation (Hobbie and Werner, 2004; Wiesenberg et al., 2004).

Upon heating at 350 °C for 1 h long-chain *n*-alkane $\delta^{13}C$ values from leaves were unaltered or only slightly altered (≤1‰) following an initial ^{13}C enrichment phase up to 150 °C and a ^{13}C depletion phase up to 250–350 °C. At 450 °C, $\delta^{13}C$ values shifted by 3–4‰. This final ^{13}C enrichment phase is in line with the preferential loss of ^{12}C-enriched CO_2 from OM upon heating (Fig. 3). These changes are consistent with other studies that have identified small changes in long-chain *n*-alkane $\delta^{13}C$ values from leaves up to hydrous pyrolysis temperature of 250 °C (≤1‰) and changes of ca. 2‰ above this temperature (Diefendorf et al., 2015). On the other hand, the mid-chain *n*-alkane $\delta^{13}C$ values showed an opposite trend up to 350 °C and a final ^{13}C enrichment phase (Fig. 3). At constant temperature (250 °C) versus time (1, 3 and 5 h) the long-chain *n*-alkane $\delta^{13}C$ values increased whereas mid-chain *n*-alkane $\delta^{13}C$ values decreased (Fig. 4).

For branch samples, the long-chain *n*-alkane $\delta^{13}C$ values from bark and xylem revealed small variations with increasing temperature whereas the mid-chain *n*-alkane $\delta^{13}C$ values decreased with charring. In bark samples there is an initial ^{13}C depletion phase up to 150 °C (≤1‰), a ^{13}C enrichment phase up to 250 °C (<2‰), and a final ^{13}C depletion phase. The long and mid-chain *n*-alkane $\delta^{13}C$ values from xylem samples were slightly altered (≤1‰) up to 350 °C except from those mid-chain *n*-alkane $\delta^{13}C$ values at 350 °C which changed with a magnitude of 2‰ (Table 2 and

Table 2
Carbon isotope values of individual *n*-alkanes in fresh and charred samples with 1 standard deviation shown for samples with 3 replicates. The $\delta^{13}C$ values are normalized to the VPDB standard.

	Celtis leaves REF	σ	*Celtis* leaves 150 °C 1 h	σ	*Celtis* leaves 250 °C 1 h	σ	*Celtis* leaves 250 °C 3 h	σ	*Celtis* leaves 250 °C 5 h	σ	*Celtis* leaves 350 °C 1 h	σ	*Celtis* leaves 450 °C 1 h	σ
$\delta^{13}C$ *n*-C_{21} (‰)	–	–	−32.1	±0.5	−32.3	±0.2	−33.0	±0.4	−32.1	±0.4	−31.3	±0.5	–	–
$\delta^{13}C$ *n*-C_{23} (‰)	−31.9	±0.4	−32.6	±0.0	−32.4	±0.2	−33.2	±0.4	−32.4	±0.2	−32.9	±0.4	–	–
$\delta^{13}C$ *n*-C_{25} (‰)	−32.2	±0.4	−32.8	±0.1	−31.8	±0.1	−32.8	±0.1	−32.5	±0.1	−33.1	±0.4	−29.3	±0.1
$\delta^{13}C$ *n*-C_{27} (‰)	−33.7	±0.5	−33.5	±0.0	−33.9	±0.3	−32.4	±0.4	−32.3	±0.4	–	–	−29.6	±0.1
$\delta^{13}C$ *n*-C_{29} (‰)	−32.9	±0.0	−32.1	±0.0	−32.8	±0.1	−32.2	±0.3	−32.7	±0.3	−32.8	±0.2	−29.5	±0.1
$\delta^{13}C$*n*-C_{31} (‰)	−33.5	±0.1	−32.2	±0.0	−32.9	±0.1	−32.2	±0.1	−32.5	±0.1	−31.6	±0.1	−29.8	±0.2
$\delta^{13}C$ *n*-C_{33} (‰)	−34.2	±0.2	−33.2	±0.0	−33.3	±0.1	−32.8	±0.1	−32.9	±0.1	−33.5	±0.2	−30.1	±0.0
Average (C_{21}. C_{23}. C_{25})	−32.0	±0.4	−32.7	±0.1	−32.1	±0.2	−33.0	±0.3	−32.4	±0.2	−33.0	±0.4	−29.3	±0.1
Average (C_{27}. C_{29}. C_{31})	−33.6	±0.2	−32.8	±0.0	−33.2	±0.1	−32.4	±0.2	−32.6	±0.2	−32.6	±0.1	−29.7	±0.1

	Celtis bark branches REF	σ	*Celtis* bark branches 150 °C1 h	σ	*Celtis* bark branches 250 °C 1 h	σ	*Celtis* bark branches 350 °C 1 h	σ	*Celtis* bark branches 450 °C 1 h	σ
$\delta^{13}C$ *n*-C_{21} (‰)	−32.0	±0.6	−33.4	±0.3	−34.1	±0.1	−33.9	±0.5	–	–
$\delta^{13}C$ *n*-C_{23} (‰)	−32.5	±0.1	−34.2	±0.3	−35.1	±0.2	−34.8	±0.2	–	–
$\delta^{13}C$ *n*-C_{25} (‰)	−36.3	±0.3	−36.4	±0.3	−35.9	±0.4	−36.3	±0.4	–	–
$\delta^{13}C$ *n*-C_{27} (‰)	−36.1	±0.5	−37.8	±0.2	−35.5	±0.2	−37.1	±0.2	–	–
$\delta^{13}C$ *n*-C_{29} (‰)	−35.7	±0.4	−35.9	±0.4	−34.8	±0.1	−36.1	±0.3	–	–
Average (C_{21}. C_{23}. C_{25})	−33.6	±0.3	−34.7	±0.3	−35.0	±0.2	−35.0	±0.4	–	–
Average (C_{27}. C_{29}. C_{31})	−35.9	±0.4	−36.9	±0.3	−35.1	±0.1	−36.6	±0.2	–	–

	Celtis xylem branches REF	σ	*Celtis* xylem branches 150 °C 1 h	σ	*Celtis* xylem branches 250 °C 1 h	σ	*Celtis* xylem branches 350 °C 1 h	σ	*Celtis* xylem branches 450 °C 1 h	σ
$\delta^{13}C$ *n*-C_{21} (‰)	−32.7	±0.4	−31.5	±0.4	−34.6	±0.5	−32.8	±0.2	–	–
$\delta^{13}C$ *n*-C_{23} (‰)	−32.1	±0.4	−31.5	±0.3	−34.6	±0.2	−33.3	±0.2	–	–
$\delta^{13}C$ *n*-C_{25} (‰)	−33.2	±0.0	−32.2	±0.1	−32.5	±0.3	−33.9	±0.1	–	–
$\delta^{13}C$ *n*-C_{27} (‰)	−32.9	±0.5	−31.4	±0.1	−32.1	±0.1	−31.4	±0.2	–	–
$\delta^{13}C$ *n*-C_{29} (‰)	−31.1	±0.4	–	–	−29.2	±0.2	–	–	–	–
Average (C_{21}. C_{23}. C_{25})	−32.7	±0.3	−31.7	±0.2	−33.9	±0.3	−33.3	±0.2	–	–
Average (C_{27}. C_{29}. C_{31})	−32.0	±0.4	−31.4	±0.1	−30.7	±0.2	−31.4	±0.2	–	–

	Celtis bark twigs REF	σ	*Celtis* bark twigs 150 °C 1 h	σ	*Celtis* bark twigs 250 °C 1 h	σ	*Celtis* bark twigs 350 °C 1 h	σ	*Celtis* bark twigs 450 °C 1 h	σ
$\delta^{13}C$ *n*-C_{21} (‰)	−34.1	±0.4	–	–	−32.7	±0.4	−31.0	±0.4	–	–
$\delta^{13}C$ *n*-C_{23} (‰)	−34.1	±0.2	–	–	−33.3	±0.4	−32.0	±0.2	–	–
$\delta^{13}C$ *n*-C_{25} (‰)	−35.0	±0.5	−35.0	±0.3	−33.2	±0.5	−34.3	±0.5	–	–
$\delta^{13}C$ *n*-C_{27} (‰)	−37.6	±0.3	−35.0	±0.1	−32.6	±0.3	−35.2	±0.4	–	–
$\delta^{13}C$ *n*-C_{29} (‰)	−36.1	±0.4	−35.1	±0.5	−31.0	±0.4	–	–	–	–
$\delta^{13}C$ *n*-C_{31} (‰)	−34.1	±0.3	−34.7	±0.5	–	–	–	–	–	–
Average (C_{21}. C_{23}. C_{25})	−34.4	±0.4	−35.0	±0.3	−33.1	±0.4	−32.5	±0.4	–	–
Average (C_{27}. C_{29}. C_{31})	−36.0	±0.3	−34.9	±0.3	−31.8	±0.3	−35.2	±0.4	–	–

	Celtis xylem twigs REF	σ	*Celtis* xylem twigs 150 °C 1 h	σ	*Celtis* xylem twigs 250 °C 1 h	σ	*Celtis* xylem twigs 350 °C 1 h	σ	*Celtis* xylem twigs 450 °C 1 h	σ
$\delta^{13}C$ *n*-C_{21} (‰)	−30.5	±0.2	−30.8	±0.1	−33.1	±0.1	−33.4	±0.2	–	–
$\delta^{13}C$ *n*-C_{23} (‰)	−32.3	±0.4	−28.5	±0.0	−33.7	±0.3	−34.4	±0.2	–	–
$\delta^{13}C$ *n*-C_{25} (‰)	−29.9	±0.4	−32.7	±0.3	–	–	–	–	–	–
$\delta^{13}C$ *n*-C_{27} (‰)	−32.3	±0.1	−33.1	±0.2	–	–	–	–	–	–
$\delta^{13}C$ *n*-C_{29} (‰)	−30.6	±0.4	−32.3	±0.5	–	–	–	–	–	–
Average (C_{21}. C_{23}. C_{25})	−30.9	±0.4	−30.7	±0.1	−33.4	±0.2	−33.9	±0.2	–	–
Average (C_{27}. C_{29}. C_{31})	−31.4	±0.2	−32.7	±0.3	–	–	–	–	–	–

REF: Reference sample; –: no data.

Fig. 3). The $\delta^{13}C$ values of the twig samples were altered with increasing temperature but not in any systematic way that we could identify (Fig. 3).

3.4. Implications for the interpretation of black sedimentary layers of open-air archaeological combustion structures

Under the assumption that charring preserves OM from microbial activity (Braadbaart and Poole, 2008; de La Rosa and Knicker, 2011; Mallol et al., 2013), the *n*-alkyl lipids and their carbon isotope values from black sedimentary layers would allow us to identify past vegetation (plant cover or wood-based fuels).

Thermal degradation under controlled laboratory conditions (limited oxygen conditions) caused changes in lipid distributions and in the *n*-alkane stable carbon isotope composition. We found that leafy materials have higher potential to preserve primary *n*-alkyl patterns than branches and twigs during thermal degradation. Primary *n*-alkyl patterns are different among leaves and wood, and among branches and twigs and the ACL_{15-33} varies significantly between leaf and wood (branches and twigs) samples. With increasing temperatures, *n*-alkane and fatty acid concentrations and CPI and ACL ratios decreased, although not uniformly, and also a different suite of aromatic compounds to more complex PAHs was recorded. The $\delta^{13}C_{alkane}$ was generally constant up to 350 °C; above this, the $\delta^{13}C_{alkane}$ changed by 3–4‰.

According to our experimental results and previous findings (e.g., Wiesenberg et al., 2009; Knicker et al., 2013; Diefendorf et al., 2015) and considering that: (1) microbial activity in buried sediments is low due to limited oxygen availability (Leahy and Colwer, 1990; Huang et al., 1997; van Bergen et al., 1998), (2) the preservation potential of biomarker fingerprints in charred OM is higher than in uncharred OM (Braadbaart and Poole, 2008; de La Rosa and Knicker, 2011), and (3) the average temperature recorded in the black sedimentary layers of experimental combustion structures is below 300 °C (Mallol et al., 2013), there is potential to identify primary *n*-alkane leaf patterns and their unaltered stable carbon isotope composition in charred OM from the black sedimentary layers. If such leaf biomarkers are present, they would further imply that the particular fire was made on leafy ground and that the constituent leaves reached a temperature of ≤350 °C. Regarding wood-based fuels, primary *n*-alkane wood patterns may be identified in black sedimentary layers subjected to low temperature combustion (≤150 °C). On the other hand, the thermal degradation in the leaf and wood samples display an even carbon numbered *n*-alkane pattern which could be used as a burning marker in combination with $\delta^{13}C_{alkanes}$ values and ACL and CPI ratios. The influence of combustion duration as observed by heating leaf samples at 250 °C during 1, 3 and 5 h revealed unaltered or slightly altered $\delta^{13}C$ values and more complex PAHs with increasing combustion time, but no major shifts in the *n*-alkane concentrations and ACL and CPI ratios. Similarly, Wolf et al. (2013) found that combustion duration on grasses and wood no has significant impact on char formation (e.g., amount of benzene polycarboxylic acids).

Median fire temperature close to 300 °C was reported for grass and forest ground fires whereas that of shrub fires is close to 500 °C (Wolf et al., 2013). Long-chain *n*-alkanes with a predominance of odd numbered *n*-alkanes were recorded in natural sediments heated at low temperatures (≤200 °C) (March et al., 2012) and in archaeological combustion structures related to fires on very humid soils, or on a stone floor (March, 2013). Formation of short-chain even carbon numbered *n*-alkanes maximizing at *n*-C_{16} or *n*-C_{18} were recorded in archaeological combustion structures (e.g., March, 2013) and in topsoils with charred OM (e.g., Eckmeier and Wiesenberg, 2009) as a biomarker of the combustion process. Eckmeier and Wiesenberg, (2009) reported temperatures between 400 and 500 °C and a non-woody source of charred OM contained in the topsoil of Mesolithic to Neolithic age, by comparison with experimental charred maize and rye (Wiesenberg et al., 2009).

Our experimental results underline that black sedimentary layers of open-air archaeological combustion structures may sometimes represent the charred topsoil (mainly leafy material) beneath combustion structures and corroborate the high preservation of charred OM in corresponding black sedimentary layers. Nevertheless, oxygen availability and microbial activity should be taken into account (Knicker et al., 2013). If microbial activity cannot be excluded, it is difficult to distinguish between thermally altered and microbial *n*-alkanes (Knicker et al., 2013). For a better understanding of organic matter composition and the processes related to the formation of combustion structures (combustion substrate or burnt residues; i.e., black and white layers) more experimental data on the thermal degradation of different anatomical parts of plants (including roots and seeds) and their lipid composition are required. Moreover, since some combustion structures could conceal signatures of animal lipids, compound-specific isotopic analysis should be incorporated to discern between plant and animal source.

4. Conclusions

We examined the charred OM from different anatomical parts of the *Celtis australis* tree (leaves, branches and twigs-bark and twigs-xylem) under laboratory-controlled conditions to identify its molecular and isotopic fingerprints. The results showed that *n*-alkyl patterns of *C. australis* leaves, branches and twigs are sufficiently different to allow their identification as components of combustion structures under low combustion temperature conditions. Thus, changes in $\delta^{13}C_{alkane}$ values could provide information about combustion temperature. Our observations should be examined for other species to determine if this is a common pattern. If so, it could help identify different types of fuel used in open-air archaeological combustion structures based on the distinction between fuel (wood) and the underlying soil substrate (mostly leaves) in combustion structure black sedimentary layers. In addition, the results show high potential of such black layers to conceal plant lipid molecules, which may be used as an excellent proxy for paleovegetation studies.

Acknowledgments

This research was supported by the ERC Consolidator Grant project PALEOCHAR – 648871. J. Volkman and two anonymous reviewers are gratefully acknowledged for their thoughtful and constructive reviews. We thank C. Hernández, J. Machado and P. Vidal-Matutano for fieldwork support.

Associate Editor—**Klaas G.J. Nierop**

References

Abdel-aal, E.I., Haroon, A.M., Mofeed, J., 2015. Successive solvent extraction and GC–MS analysis for the evaluation of the phytochemical constituents of the filamentous green alga *Spirogyra longata*. The Egyptian Journal of Aquatic Research 41, 233–246.

Adams, R.P., Wright, J.W., 2012. Alkanes and terpenes in wood and leaves of *Pinus jeffreyi* and *P. sabiniana*. Journal of Essential Oil Research 24, 435–440.

Aldeias, V., Dibble, H.L., Sandgathe, D., Goldberg, P., McPherron, S.J.P., 2016. How heat alters underlying deposits and implications for archaeological fire features: a controlled experiment. Journal of Archaeological Science 67, 64–79.

Alewell, C., Birkholz, A., Meusburger, K., Schindler-Wildhaber, Y., Mabit, L., 2016. Quantitative sediment source attribution with compound-specific isotope analysis in a C3 plant-dominated catchment (central Switzerland). Biogeosciences 13, 1587–1596.

Allué, E., Cáceres, I., Expósito, I., Canals, A., Rodríguez, A., Rosell, J., Bermúdez de Castro, J.M., Carbonell, E., 2015. *Celtis* remains from the Lower Pleistocene of

Gran Dolina, Atapuerca (Burgos, Spain). Journal of Archaeological Science 53, 570–577.
Ascough, P., Bird, M.I., Wormald, P., Snape, C.E., Apperley, D., 2008. Influence of pyrolysis variables and starting material on charcoal stable isotopic and molecular characteristics. Geochimica et Cosmochimica Acta 72, 6090–6102.
Badoni, R., Semwal, D.K., Rawat, U., 2010. Fatty acid composition and antimicrobial activity of *Celtis australis* L. fruits. Journal of Scientific Research 2, 397–402.
Bhattacharya, S., Dutta, S., Summons, R.E., 2017. A distinctive biomarker assemblage in an Infracambrian oil and source rock from western India: molecular signatures of eukaryotic sterols and prokaryotic carotenoids. Precambrian Research 290, 101–112.
Bianchi, G., 1994. Plant waxes. In: Hamilton, R.J. (Ed.), Waxes: Chemistry, Molecular Biology and Functions. The Oily Press, Dundee, pp. 175–222.
Braadbaart, F., Poole, I., 2008. Morphological, chemical and physical changes during charcoalification of wood and its relevance to archaeological contexts. Journal of Archaeological Science 35, 2434–2445.
Bray, E.E., Evans, E.D., 1961. Distribution of *n*-paraffins as a clue to recognition of source beds. Geochimica et Cosmochimica Acta 22, 2–15.
Bush, R.T., McInerney, F.A., 2015. Influence of temperature and C4 abundance on *n*-alkane chain length distributions across the central USA. Organic Geochemistry 79, 65–73.
Bühring, S.I., Ehrenhauss, S., Kamp, A., Moodley, L., Witte, U., 2006. Enhanced benthic activity in sandy sublittoral sediments: evidence from ^{13}C tracer experiments. Marine Biology Research 2, 120–129.
Campo, J., Nierop, K.G.J., Cammeraat, E., Andreu, V., Rubio, J.L., 2011. Application of pyrolysis-gas chromatography/mass spectrometry to study changes in the organic matter of macro- and microaggregates of a Mediterranean soil upon heating. Journal of Chromatography A 1218, 4817–4827.
Cert, A., Lanzón, A., Carelli, A.A., Albi, T., Amelotti, G., 1994. Formation of stigmasta-3,5-diene in vegetable oils. Food Chemistry 49, 287–293.
Collins, J.A., Andrez, S., Carr, A.S., Schefuß, E., Boom, A., Sealy, J., 2017. Investigation of organic matter and biomarkers from Diepkloof Rock Shelter, South Africa: insights into middle stone age site usage and palaeoclimate. Journal of Archaeological Science 85, 51–65.
Costa, M., Morla, C., Sainz, H., 1998. Los bosques Ibéricos. Editorial Planeta, Barcelona.
Cranwell, P.A., 1973. Chain-length distribution of *n*-alkanes from lake sediments in relation to postglacial environmental change. Freshwater Biology 3, 259–265.
Cranwell, P., 1981. Diagenesis of free and bound lipids in terrestrial detritus deposited in a lacustrine sediment. Organic Geochemistry 3, 79–89.
de la Rosa, J.M., Knicker, H., 2011. Bioavailability of N released from N-rich pyrogenic organic matter: an incubation study. Soil Biology and Biochemistry 43, 2368–2373.
Demır, F., Doğan, H., Özcan, M., Haciseferoğullari, H., 2002. Nutritional and physical properties of hackberry (*Celtis australis* L.). Journal of Food Engineering 54, 241–247.
Diefendorf, A.F., Freeman, K.H., Wing, S.L., Graham, H.V., 2011. Production of *n*-alkyl lipids in living plants and implications for the geologic past. Geochimica et Cosmochimica Acta 75, 7472–7485.
Diefendorf, A.F., Sberna, D.T., Taylor, D.W., 2015. Effect of thermal maturation on plant-derived terpenoids and leaf wax *n*-alkyl components. Organic Geochemistry 89–90, 61–70.
Diefendorf, A.F., Freimuth, E.J., 2017. Extracting the most from terrestrial plant-derived *n*-alkyl lipids and their carbon isotopes from the sedimentary record: a review. Organic Geochemistry 103, 1–21.
Dove, H., Mayes, R.W., Freer, M., 1996. Effect of species, plant part, and plant age on the *n*-alkane concentrations in the cuticular wax of pasture plants. Australian Journal of Agricultural Research 47, 1333–1347.
Duan, Y., Ma, L., 2001. Lipid geochemistry in a sediment core from Ruoergai Marsh deposit (Eastern Qinghai-Tibet plateau, China). Organic Geochemistry 32, 1429–1442.
Đurovic, S., Zeković, Z., Šorgić, S., Popov, S., Vujanović, M., Radojković, M., 2018. Fatty acid profile of stinging leaves: application of modern analytical procedures for sample preparation and analysis. Analytical Methods 10, 1080–1087.
Eckmeier, E., Wiesenberg, G.L.B., 2009. Short-chain *n*-alkanes (C_{16-20}) in ancient soil are useful molecular markers for prehistoric biomass burning. Journal of Archaeological Science 36, 1590–1596.
Eglinton, G., Hamilton, R.J., 1967. Leaf epicuticular waxes. Science 156, 1322–1335.
Ehleringer, J.R., Buchmann, N., Flanagan, L.B., 2000. Carbon isotope ratios in belowground carbon cycle processes. Ecological Applications 10, 412–422.
Ellis, G.P., 1959. The maillard reaction. In: Wolfrom, M.L. (Ed.), Advances in Carbohydrate Chemistry. Academic Press, New York, pp. 63–134.
Fernández, I., Cabaneiro, A., Carballas, T., 1997. Organic matter changes immediately after a wildfire in an atlantic forest soil and comparison with laboratory soil heating. Soil Biology and Biochemistry 29, 1–11.
Ficken, K.J., Li, B., Swain, D.L., Eglinton, G., 2000. An *n*-alkane proxy for the sedimentary input of the submerged/floating freshwater aquatic macrophytes. Organic Geochemistry 31, 745–749.
Fine, P., Cass, G.R., Simoneit, B.R.T., 2001. Chemical characterization of fine particle emissions from fireplace combustion of woods grown in the northeastern United States. Environmental Science and Technology 35, 2665–2675.
Freeman, K.H., Pancost, R.D., 2014. Biomarkers for terrestrial plants and climate. In: Turekian, H.D., Holland, K.K. (Eds.), Treatise on Geochemistry. Elsevier, pp. 395–416.
Fu, P.Q., Kawamura, K., Chen, J., Charrière, B., Sempéré, R., 2013. Organic molecular composition of marine aerosols over the Arctic Ocean in summer: contributions of primary emission and secondary aerosol formation. Biogeosciences 10, 653–667.
Gamarra, B., Kahmen, A., 2015. Concentrations and δ^2H values of cuticular *n*-alkanes vary significantly among plant organs, species and habitats in grasses from an alpine and a temperate European grassland. Oecologia 178, 981–998.
García Moreno, A., Rios Garaizar, J., Marín Arroyo, A.B., Eugenio Ortíz, J., de Torres, T., López-Dóriga, I., 2014. La secuencia musteriense de la Cueva del Niño (Aýna, Albacete) y el poblamiento neandertal en el sureste de la península Ibérica. Trabajos de Prehistoria 71, 221–241.
Gocke, M., Kuzyakov, Y., Wiesenberg, G.L.B., 2011. Differentiation of plant derived organic matter in soil, loess and rhizoliths based on *n*-alkane molecular proxies. Biogeochemistry 112, 23–40.
Hobbie, E.A., Werner, R., 2004. Intramolecular, compound-specific, and bulk carbon isotope patterns in C3 and C4 plants: a review and synthesis. New Phytologist 161, 371–385.
Huang, Y.S., Eglinton, G., Ineson, P., Latter, P.M., Bol, R., Harkness, D.D., 1997. Absence of carbon isotope fractionation of individual *n*-alkanes in a 23-year field decomposition experiment with *Calluna vulgaris*. Organic Geochemistry 26, 273–287.
Huang, X., Wang, C., Zhang, J., Wiesenberg, G., Zhang, Z., Xie, S., 2011. Comparison of free lipid compositions between roots and leaves of plants in the Dajiuhu Peatland, central China. Geochemical Journal 45, 365–373.
Ihara, S., Tanaka, T., 1978. Fatty acid compositions of the oils of *Celtis sinensis var. japonica* and *Zelkova serrata*. Journal of the American Oil Chemists Society 55, 471–472.
Jambrina-Enríquez, M., Sachse, D., Valero-Garcés, B.L., 2016. A deglaciation and Holocene biomarker-based reconstruction of climate and environmental variability in NW Iberian Peninsula: the Sanabria Lake sequence. Journal of Paleolimnology 56, 49–66.
Jansen, B., Nierop, K., Hageman, J., Cleef, A.M., Verstraten, J.M., 2006. The straight-chain lipid biomarker composition of plant species responsible for the dominant biomass production along two altitudinal transects in the Ecuadorian Andes. Organic Geochemistry 37, 514–1536.
Jansen, B., Nierop, K.G.J., Tonneijck, F.H., van der Wielen, F.W.M., Verstraten, J.M., 2007. Can isoprenoids in leaves and roots of plants along altitudinal gradients in the Ecuadorian Andes serve as biomarkers? Plant and Soil 291, 181–198.
Jansen, B., Wiesenberg, G.L.B., 2017. Opportunities and limitations related to the application of plant-derived lipid molecular proxies in soil science. Soil 3, 211–234.
Kaal, J., Martínez Cortizas, A., Reyes, O., Soliño, M., 2012. Molecular characterization of *Ulex europaeus* biochar obtained from laboratory heat treatment experiments – a pyrolysis–GC/MS study. Journal of Analytical and Applied Pyrolysis 95, 205–212.
Kawamura, K., Ishimura, Y., Yamazaki, K., 2003. Four years' observations of terrestrial lipid class compounds in marine aerosols from the western North Pacific. Global Biogeochemical Cycles 17, 1003. https://doi.org/10.1029/2001GB001810.
Keiluweit, M., Kleber, M., Sparrow, M.A., Simoneit, B.R.T., Prahl, F.G., 2012. Solvent extractable polycyclic aromatic hydrocarbons in biochar: influence of pyrolysis temperature and feedstock. Environmental Science and Technology 46, 9333–9341.
Knicker, H., Hilscher, A., De la Rosa, J., González-Pérez, J., González-Vila, F.J., 2013. Modification of biomarkers in pyrogenic organic matter during the initial phase of charcoal biodegradation in soils. Geoderma 197–198, 43–50.
Kuo, L.J., Herbert, B.E., Louchouarn, P., 2008. Can levoglucosan be used to characterize and quantify char/charcoal black carbon in environmental media? Organic Geochemistry 39, 1466–1478.
Leahy, J.C., Colwer, R.R., 1990. Microbial degradation of hydrocarbons in the environment. Microbiological Reviews 54, 305–315.
Leroi-Gourhan, A., 1973. Séminaire sur les structures d'habitat: témoins de combustion. Collège de France, Paris.
Liu, K.S., 1994. Preparation of fatty acid methyl esters for gas-chromatographic analysis of lipids in biological materials. Journal of the American Oil Chemists Society 71, 1179–1187.
Mallol, C., Hernández, C.M., Cabanes, D., Sistiaga, A., Machado, J., Rodríguez, A., Pérez, L., Galván, B., 2013. The black layer of Middle Palaeolithic combustion structures. Interpretation and archaeostratigraphic implications. Journal of Archaeological Science 40, 2515–2537.
Mallol, C., Mentzer, S., Miller, C., 2017. Combustion features. In: Nicosia, C., Stoops, G. (Eds.), Archaeological Soil and Sediment Micromorphology. Wiley, pp. 299–326.
March, R., 2013. Searching for the functions of fire structures in Eynan (Mallaha) and their formation processes: a geochemical approach. In: Bar-Yosef, O., Valla, F.R. (Eds.), Natufian Foragers in the Levant Terminal Pleistocene - Social Changes in Western Asia. International Monographs in Prehistory Archaeological Series 19(17). Ann Arbor, Michigan U.S.A., pp. 227–284.
March, R.J., Lucquin, A., Joly, D., Ferreri, J.C., Muhieddine, M., 2012. Processes of formation and alteration of archaeological fire structures: complexity viewed in the light of experimental approaches. Journal of Archaeological Method and Theory 21, 1–45.
Marynowski, L., Kubik, R., Uhl, D., Simoneit, B.R.T., 2014. Molecular composition of fossil charcoal and relationship with incomplete combustion of Word. Organic Geochemistry 77, 22–31.

Mastelic, J., Jerkovic, I., Mesis, M., 2006. Volatile constituents from flowers, leaves, bark and wood of *Prunus mahaleb* L. Flavour and fragrance Journal 21, 306–313.
Messager, E., Badou, A., Fröhlich, F., Deniauz, B., Lordkipanidze, D., Voinchet, P., 2010. Fruit and seed biomineralization and its effect on preservation. Archaeological and Anthropological Sciences 2, 25–34.
Meyers, P.A., 2003. Applications of organic geochemistry to paleolimnological reconstructions: a summary of examples from the Laurentian Great Lakes. Organic Geochemistry 34, 261–289.
O'Malley, V.P., Burke, R.A., Schlotzhauer, W.S., 1997. Using GC-MS/Combustion/IRMS to determine the $^{13}C/^{12}C$ ratios of individual hydrocarbons produced from the combustion of biomass materials–application to biomass burning. Organic Geochemistry 27, 567–581.
Oros, D.R., Simoneit, B.R.T., 2001a. Identification and emission factors of molecular tracers in organic aerosols from biomass burning: Part 1. Temperate climate conifers. Applied Geochemistry 16, 1513–1544.
Oros, D.R., Simoneit, B.R.T., 2001b. Identification and emission factors of molecular tracers in organic aerosols from biomass burning: Part 2. Deciduous trees. Applied Geochemistry 16, 1545–1565.
Ota, A., Višnjevec, A.M., Vidrih, R., Prgomet, Ž., Nečemer, M., Hribar, J., Comerman, N. G., Možina, S.S., Bučar-Miklavčič, M., Ulrih, N.P., 2017. Nutritional, antioxidative, and antimicrobial analysis of the Mediterranean hackberry (*Celtis australis* L.). Food Science and Nutrition 5, 160–170.
Post-Beittenmiller, D., 1996. Biochemistry and molecular biology of wax production in plants. Annual Review of Plant Physiology and Plant Molecular Biology 47, 405–430.
Pu, Y., Wang, C., Meyers, P., 2017. Origins of biomarker aliphatic hydrocarbons in sediments of alpine Lake Ximencuo, China. Palaeogeography, Palaeoclimatology, Palaeoecology 475, 106–114.
Rieley, G., Collier, R.J., Jones, D.M., Eglinton, G., 1991. The biogeochemistry of Ellesmere Lake, U.K.—1: source correlation of leaf wax inputs to the sedimentary lipid record. Organic Geochemistry 17, 901–912.
Rowland, R.L., 1957. Flue-cured tobacco II. Neophytadiene. Journal of the American Chemical Society 79, 5007–5010.
Rushdi, A.I., Simoneit, B.R.T., DouAbul, A.A.Z., Al-Mutlaq, K.F., El-Mubarak, A.H., Qurban, M., Goñi, M.A., 2014. Occurrence and sources of polar lipid tracers in sediments from the Shatt al-Arab River of Iraq and the northwestern Arabian Gulf. Science of The Total Environment 470–471, 180–192.
Rushdi, A.I., DouAbul, A.A.Z., Al-Maarofi, S.S., Simoneit, B.R.T., 2018. Impacts of Mesopotamian wetland re-flooding on the lipid biomarker distributions in sediments. Journal of Hydrology 558, 20–28.
Sachse, D., Radke, J., Gleixner, G., 2004. Hydrogen isotope ratios of recent lacustrine sedimentary *n*-alkanes record modern climate variability. Geochimica et Cosmochimica Acta 68, 4877–4889.
Santa-Cruz, L.H., Turner, C.E., Knapp, J.E., Schiff, P.L., Slatkin, D.J., 1975. Moretenol and other constituents of *Celtis laevigata*. Phytochemistry 4, 2532–2533.
Sañé, E., Isla, E., Pruski, A.M., Bárcena, M.A., Vétion, G., DeMaster, D., 2011. Diatom valve distribution and sedimentary fatty acid composition in Larsen Bay, Eastern Antarctica Peninsula. Continental Shelf Research 31, 1161–1168.
Schnell, G., Schaeffer, P., Tardivon, H., Motsch, E., Connan, J., Ertlen, D., Schwartz, D., Schneider, N., Adam, P., 2014. Contrasting diagenetic pathways of higher plant triterpenoids in buried wood as a function of tree species. Organic Geochemistry 66, 107–124.
Schwark, L., Zink, K., Lechterbeck, J., 2002. Reconstruction of postglacial to early Holocene vegetation history in terrestrial Central Europe via cuticular lipid biomarkers and pollen records from lake sediments. Geology 30, 463–466.
Semwal, R.B., Semwal, D.K., 2012. Analgesic and anti-inflammatory activities of extracts and fatty acids from *Celtis australis* L. The Natural Products Journal 2, 323–327.
Simoneit, B.R.T., Mazurek, M.A., 1982. Organic matter of the troposphere—II. Natural background of biogenic lipid matter in aerosols over the rural western United States. Atmospheric Environment 16, 2139–2159.
Simoneit, B.R.T., 2002. Biomass burning – a review of organic tracers for smoke from incomplete combustion. Applied Geochemistry 17, 129–162.
Smith, D.G., Mayes, R.W., Raats, J.G., 2001. Effect of species, plant part, and season of harvest on *n*-alkane concentrations in the cuticular wax of common rangeland grasses from southern Africa. Australian Journal of Agricultural Research 52, 875–882.
Sytsma, K.J., Morawetz, G., Pires, J.C., Nepokroeff, M., Conti, E., Zjhra, M., Hall, J.C., Chase, M.W., 2002. *Urticalean rosids*: circumscription, rosid ancestry, and phylogenetics based on *rbcL*, *trnL-F*, and *ndhF* sequences. American Journal of Botany 89, 1531–1546.
Tutin, T.G., Heywood, V.H., Burges, N.A., Valentine, D.H., Walters, S.M., Webb, D.A. (Eds.), 1964. Flora Europaea. Lycopodiaceae to Platanaceae, vol. 1. Cambridge University Press, Cambridge.
van Bergen, P.F., Nott, C.J., Bull, I.D., Poulton, P.R., Evershed, R.P., 1998. Organic geochemical studies of soils from the Rothamsted classical experiments – IV. Preliminary results from a study of the effect of soil pH on organic matter decay. Organic Geochemistry 29, 1779–1795.
Venkata, R.B., Samuel, L.A., Pardha, S.M., Narashimha, R.B., Krishna, N.V., Sudhakar, M., Radhakrishnan, T.M., 2012. Antibacterial, antioxidant activity and GC–MS analysis of *Eupatorium odoratum*. Asian Journal of Pharmaceutical and Clinical Research 5, 99–106.
Vidal-Matutano, P., Pérez-Jordà, G., Hernández, C.M., Galván, B., 2018. Macrobotanical evidence (wood charcoal and seeds) from the Middle Palaeolithic site of El Salt, Eastern Iberia: palaeoenvironmental data and plant resources catchment areas. Journal of Archaeological Science: Reports 19, 454–464.
Wang, M., Zhang, W., Hou, J., 2015. Is average chain length of plant lipids a potential proxy for vegetation, environment and climate changes? Biogeosciences Discussions 12, 5477–5501.
Wiedemeier, D.B., Brodowski, S., Wiesenberg, G.L.B., 2015. Pyrogenic molecular markers: linking PAH with BPCA analysis. Chemosphere 119, 432–437.
Wiesenberg, G.L.B., Schwark, L., 2006. Carboxylic acid distribution patterns of temperate C3 and C4 crops. Organic Geochemistry 37, 1973–1982.
Wiesenberg, G.L.B., Schwarzbauer, J., Schmidt, M.W.I., Schwark, L., 2004. Source and turnover of organic matter in agricultural soils derived from *n*-alkane/*n*-carboxylic acid compositions and C-isotope signatures. Organic Geochemistry 35, 1371–1393.
Wiesenberg, G., Lehndorff, E., Schwark, L., 2009. Thermal degradation of rye and maize straw: lipid pattern changes as a function of temperature. Organic Geochemistry 40, 167–174.
Wolf, M., Lehndorff, E., Wiesenberg, G.L.B., Stockhausen, M., Schwark, L., Amelung, W., 2013. Towards reconstruction of past fire regimes from geochemical analysis of charcoal. Organic Geochemistry 55, 11–21.
Yunker, M.B., Macdonald, R.W., Vingarzan, R., Mitchel, R.H., Goyette, D., Sylvestre, S., 2002. PAHs in the Fraser River basin: a critical appraisal of PAH ratios as indicators of PAH source and composition. Organic Geochemistry 33, 489–515.